A 3D brain unit model to further improve prediction of local drug distribution within the brain

Esmée Vendel [1], Vivi Rottschäfer [1*], Elizabeth C. M. de Lange [2*]

1 Mathematical Institute, Leiden University, Leiden, The Netherlands
2 Leiden Academic Centre for Drug Research, Leiden University, Leiden, The Netherlands

* vivi@math.leidenuniv.nl, ecmdelange@lacdr.leidenuniv.nl

Abstract

The development of drugs targeting the brain still faces a high failure rate. One of the reasons is a lack of quantitative understanding of the complex processes that govern the pharmacokinetics (PK) of a drug within the brain. While a number of models on drug distribution into and within the brain is available, none of these addresses the combination of factors that affect local drug concentrations in brain extracellular fluid (brain ECF).
Here, we develop a 3D brain unit model, which builds on our previous proof-of-concept 2D brain unit model, to understand the factors that govern local unbound and bound drug PK within the brain. The 3D brain unit is a cube, in which the brain capillaries surround the brain ECF. Drug concentration-time profiles are described in both a blood-plasma-domain and a brain-ECF-domain by a set of differential equations. The model includes descriptions of blood plasma PK, transport through the blood-brain barrier (BBB), by passive transport via paracellular and trancellular routes, and by active transport, and drug binding kinetics. The impact of all these factors on ultimate local brain ECF unbound and bound drug concentrations is assessed.
In this article we show that all the above mentioned factors affect brain ECF PK in an interdependent manner. This indicates that for a quantitative understanding of local drug concentrations within the brain ECF, interdependencies of all transport and binding processes should be understood. To that end, the 3D brain unit model is an excellent tool, and can be used to build a larger network of 3D brain units, in which the properties for each unit can be defined independently to reflect local differences in characteristics of the brain.

Author summary

Insights on how a drug distributes within the brain over both time and space are still limited. Here, we develop a '3D brain unit model' in order to understand the factors that control drug concentrations within a small piece of brain tissue, the 3D brain unit. In one 3D brain unit, the brain capillaries, which are the smallest blood vessels of the brain, surround the brain extracellular fluid (ECF). The blood-brain barrier (BBB) is located between the brain capillaries and the brain ECF. The model describes the impact of brain capillary blood flow, transport across the BBB, diffusion, flow and drug binding on the distribution of a drug within the brain ECF. We distinguish between free (unbound) drug and drug that is bound to binding sites within the brain. We show that

all of the above mentioned factors affect drug concentrations within brain ECF in an interdependent manner. The 3D brain unit model that we have developed is an excellent tool to increase our understanding of how local drug concentrations within the brain ECF are affected by brain transport and binding processes.

1 Introduction

The brain capillary bed is the major site of drug exchange between the blood and the brain. Blood flows from the general blood circulation into the brain capillary bed by a feeding arteriole and back by a draining venule. The rate at which drug molecules within the blood are exposed to the brain is determined by the brain capillary blood flow rate. Drug exchange between the blood plasma in the brain capillaries and the brain extracellular fluid (ECF) is controlled by the blood-brain barrier (BBB).
Drug distribution into and within the brain has been extensively summarized in a recent review [1]. In short, the BBB has great impact on the relationship between the concentration-time profiles of unbound drug in the blood plasma (blood plasma pharmacokinetics (PK)) and in the brain ECF (brain ECF PK). The BBB consists of brain endothelial cells that are held closely together by tight junctions. Unbound drug may cross the BBB by passive and/or active transport [2–10]. Passive transport is bidirectional and occurs by diffusion through the BBB endothelial cells (transcellular transport) and through the BBB tight junctions (paracellular transport). Active transport is unidirectional and can be directed inward (from the blood plasma to the brain ECF, active influx) or outward (from the brain ECF to the blood plasma, active efflux). Once having crossed the BBB, drug distributes within the brain ECF by diffusion. Diffusion within the brain ECF is hindered by the brain cells [11, 12]. This hindrance is described by the so-called tortuosity and leads to an effective diffusion that is smaller than normal (in a medium without obstacles). Moreover, a fluid flow, the brain ECF bulk flow, is present. The brain ECF bulk flow results from the generation of brain ECF by the BBB and drainage into the cerebrospinal fluid (CSF). Both diffusion and brain ECF bulk flow are important for the distribution of a drug to its target site, which is the site where a drug exerts its effect. In order to do induce an effect, a drug needs to bind to specific binding sites (targets). Only unbound drug, i.e. drug that is not bound to any components of the brain, can interact with its target [13, 14]. This is a dynamic process of association and dissociation, the so-called drug binding kinetics. These association and dissociation rates may affect the concentration of unbound drug at the target site [15, 16]. While the drug dissociation rate has been thought of as the most important determinant of the duration of interactions between a drug and its binding site [17], a more recent study shows that the drug association rate is equally important [16].
A number of models integrating several of the discussed processes of drug distribution into and within the brain is available, see for example [11, 12, 18–25] and [26]. The most recent and comprehensive brain drug distribution model is the physiologically-based pharmacokinetic model for the rat and for human [27, 28]. This model takes multiple compartments of the central nervous system (CNS) into account, including plasma PK, passive paracellular and transcellular BBB transport, active BBB transport, and distribution between the brain ECF, intracellular spaces, and multiple CSF sites, on the basis of CNS-specific and drug-specific parameters. However, it does not take into account distribution within brain tissue (brain ECF).
Here, we developed a 3D brain unit model, in which local brain drug distribution is explicitly taken into account. The 3D brain unit model encompasses blood plasma PK, the BBB, brain ECF, brain ECF bulk flow, diffusion, and binding to specific and non-specific binding sites within the brain. This 3D piece of brain tissue can be

considered the smallest physiological unit of the brain in terms of drug transport. Within the 3D brain unit, drug is carried along with the blood plasma by the brain capillary blood flow and as such presented to the brain ECF. Drug distributes between the blood plasma and the brain ECF by transport across the BBB. Thereafter, drug distribution within the brain ECF is affected by diffusion, bulk flow and binding. We describe the distribution of drug within the brain ECF by a partial differential equation (PDE) and couple this to two ordinary differential equations (ODEs) to account for specific and non-specific drug binding.

The model builds on a proof-of-concept 2D brain unit model [29]. The 2D model is a basic model covering many essential aspects of drug distribution within the brain, including passive BBB transport, diffusion, brain ECF bulk flow, specific binding of a drug at its target site and non-specific binding of a drug to components of the brain. Here, brain cells are implicitly implemented by describing the hindrance the cells impose on the transport of a drug within the brain ECF in a tortuosity term. This model has enabled the study of the effect of drug properties and brain tissue characteristics on the distribution of a drug within the brain ECF and on its specific and non-specific binding behaviour of the drug.

The current *3D* brain unit model further improves the prediction of drug distribution within the brain. The third dimension improves the realistic features of the model as the brain is also 3D. Then, the brain capillary blood flow and active transport across the BBB, which are both important mechanisms of drug transport into the brain, are included. Here, we focus on one single brain unit. This allows for a thorough characterisation of drug distribution within one 3D brain unit before expanding to a larger scale.

In the remainder of this article, the mathematical representation of the characteristics of the 3D brain unit is introduced (section 2). There, we formulate the model (section 2.1) and the mathematical descriptions of the drug distribution within the blood plasma of the brain capillaries (section 2.2) and within the brain (section 2.3). In section 2.4 we formulate the model boundary conditions that describe drug exchange between the blood plasma and the brain ECF by passive and active BBB transport, as well as drug transport at the boundaries of the unit. In section 3, we study the effect of several factors on drug distribution within the brain ECF. In section 3.1, we evaluate the effect of the brain capillary blood flow velocity on local brain ECF PK in the 3D brain unit. Next, we evaluate the effect of active influx and efflux on local brain ECF PK (section 3.2). Then, in section 3.3 we show how the interplay between the brain capillary blood flow velocity, passive BBB permeability and active transport affects drug concentrations within the 3D brain unit. Finally, in section 4 we conclude our work and discuss future perspectives.

2 The 3D brain unit

The 3D brain unit represents the smallest piece of brain tissue that contains all physiological elements of the brain. The 3D brain unit is part of a larger network of 3D brain units, but here we focus on just one 3D brain unit that is fed by an arteriole and drained by a venule (Fig 1, left). The 3D brain unit is a cube in which the brain capillaries (represented by red rectangular boxes on the ribs) surround the brain ECF (Fig 1, left). The segments of red rectangular boxes protruding from the vertices from the 3D brain unit are parts of brain capillaries from neighbouring units. As such, each vertex connects three incoming brain capillaries to three outgoing brain capillaries, with the exception of the vertex connected to the arteriole and the vertex connected to the venule. These connect the arteriole to three outgoing brain capillaries and three incoming brain capillaries to the venule, respectively. A single 3D brain unit (Fig 1,

Fig 1. Sketch of the 3D model brain unit. Left: The structure represented by the 3D brain unit. An arteriole carries blood plasma (containing drug) into a brain capillary bed, that is connected to a venule that drains the blood plasma. The brain capillaries (red) surround the brain ECF (blue). Middle: the 3D brain unit and its sub-domains. The unit consists of a brain-ECF-domain (blue) and a blood-plasma-domain (red). The blood-plasma-domain is divided into several subdomains: U_{in} is the domain where the dose of absorbed drug enters the 3D brain unit, $U_{\text{x1-x4}}$, $U_{\text{y1-y4}}$ and $U_{\text{z1-z4}}$ are the domains representing the x-directed, y-directed and z-directed capillaries, respectively. Right: Directions of transport in the model. The drug enters the brain capillaries in U_{in}. From there, it is transported through the brain capillaries by the brain capillary blood flow in the direction indicated by the small arrows. Drug in the brain capillary blood plasma exchanges with the brain ECF by crossing the BBB. Drug within the brain ECF is, next to diffusion, transported along with brain ECF bulk flow (indicated by the bold arrow).

middle) has a blood-plasma-domain (red) consisting of multiple sub-domains. These include the brain capillary domain where drug enters the unit (indicated by U_{in} in Fig 1), the domains representing the x-directed, y-directed and z-directed brain capillaries (indicated by $U_{\text{x1}-\text{x4}}$, $U_{\text{y1}-\text{y4}}$ and $U_{\text{z1}-\text{z4}}$ in Fig 1) and the brain capillary domain where drug leaves the unit (indicated by U_{out} in Fig 1). Drug within the blood plasma is transported by the brain capillary blood flow. The brain capillary blood flow splits at the vertices of the unit, where brain capillary branching occurs (Fig 1, right).
In developing the model, we make the following assumptions about drug distribution within the brain capillaries:

Assumptions 1.

(i) *The drug concentration within the blood plasma changes over time as a function of the rates of absorption (in case of oral administration) and elimination into and from the blood plasma.*

(ii) *The blood carrying the drug flows into 3D brain unit by a feeding arteriole and leaves via a draining venule (Fig 1, left).*

(iii) *The drugs enters the brain unit in the domain U_{in} (Fig 1, middle).*

(iv) *The brain capillary blood flow is directed away from U_{in} (Fig 1, right).*

(v) *Diffusion within the blood plasma is negligible compared to the brain capillary blood flow, hence drug is transported through the brain capillaries solely by the brain capillary blood flow.*

(vi) *The brain capillaries are all equal in size and surface area. In addition, we assume that the volume of the incoming arteriole equals the volume of the three outgoing brain capillaries it connects to and that the volume of the outgoing venule equals the volume of the three incoming brain capillaries it connects to. Consequently, as the total volume of incoming blood vessels equals the total volume of outgoing blood vessels at each vertex (see Fig 1, left), the brain capillary blood flow velocity is by default equal in all brain capillaries.*

(vii) *Drug within the blood plasma does not bind to blood plasma proteins. All drug within the blood plasma is in an unbound state and is able to cross the BBB.*

Drug within the blood plasma of the brain capillaries crosses the BBB to exchange with the brain ECF. The BBB is located at the border between the brain capillaries (red) and the brain ECF (blue), see Fig 1. Drug exchange between the blood plasma and the brain ECF is described by passive and active transport across the BBB in both directions.

Within the brain ECF, we formulate:

Assumptions 2.

(i) *Drug within the brain ECF is transported by diffusion and brain ECF bulk flow.*

(ii) *Cells are not explicitly considered, but only by taking the tortuosity (hindrance on diffusion imposed by the cells) into account.*

(iii) *The brain ECF bulk flow is unidirectional. It is pointed in the x-direction, see the*

Fig 2. Front view of the 3D brain unit. Definitions of U_{pl} are given. The x-directed, y-directed and z-capillaries are divided by the lines x=y (or y=z or x=z) and x+y=y_r (or y+z=z_r or x+z=z_r). The only exceptions for this are the brain capillaries adjacent to U_{in} and the brain capillaries adjacent to U_{out}.

bold arrow in Fig 1 (right).
(iv) *All drug distributes within the brain ECF and we only have extracellular binding sites.*
(v) *The total concentration of specific and non-specific binding sites is constant.*
(vi) *The specific and non-specific binding sites are evenly distributed over the 3D brain unit and do not change position.*
(vii) *The specific and non-specific binding sites lie on the outside of cells and the drug does not have to cross cell membranes in order to bind to binding sites.*
(viii) *Drug binding is reversible and drugs associate and dissociate from their binding sites.*

2.1 Formulation of the 3D brain unit

The 3D brain unit is a cubic domain, U, that represents a piece of brain tissue. We define $\mathrm{U} = \{(\mathrm{x,y,z}) \in \mathbb{R}^3 \mid 0 \leq \mathrm{x} \leq \mathrm{x_r} \wedge 0 \leq \mathrm{y} \leq \mathrm{y_r} \wedge 0 \leq \mathrm{z} \leq \mathrm{z_r}\}$. There, $\mathrm{x_r}$, $\mathrm{y_r}$ and $\mathrm{z_r}$ are constants that represent the length of one unit, which is then defined as $d_{\mathrm{cap}}+2r$, with d_{cap} the distance between the brain capillaries and r the brain capillary radius. In one brain unit, the brain capillaries, the BBB and the brain ECF are represented by the subsets $U_{\mathrm{pl}} \subset U$, $U_{\mathrm{BBB}} \subset U$ and $U_{\mathrm{ECF}} \subset U$, respectively, such that $U = U_{\mathrm{pl}} \cup U_{\mathrm{BBB}} \cup U_{\mathrm{ECF}}$.
Within U_{pl}, we define U_{in} as the domain where the blood plasma, containing drug, enters the 3D brain unit from a feeding arteriole. We define U_{out} as the domain where the blood plasma, containing drug, leaves the 3D brain unit to a draining venule. Additionally, we define the x-directed, y-directed and z-capillaries as the sets $\{U_{\mathrm{xi}}, \mathrm{i=1,..,4}\}$, $\{U_{\mathrm{yi}}, \mathrm{i=1,..,4}\}$ and $\{U_{\mathrm{zi}}, \mathrm{i=1,..,4}\}$. The brain capillaries are divided by the lines x=y (or y=z or x=z) and x+y=y_r (or y+z=z_r or x+z=z_r), for which an example is shown in Fig 2. The only exceptions for this are the brain capillaries adjacent to U_{in} and U_{out}, see below. The regions are defined are as follows:

$U_{\mathrm{x1}} = \{(\mathrm{x,y,z}) \in U \mid \mathrm{r} \leq \mathrm{x} < \mathrm{x_r}\text{-y},\ \mathrm{r} \leq \mathrm{x} < \mathrm{x_r}\text{-z} \wedge 0 \leq \mathrm{y} < \mathrm{r} \wedge 0 \leq \mathrm{z} < \mathrm{r}\}$
$U_{\mathrm{x2}} = \{(\mathrm{x,y,z}) \in U \mid \mathrm{y_r}\text{-y} < \mathrm{x} \leq \mathrm{y} \wedge \mathrm{z} \leq \mathrm{x} < \mathrm{x_r}\text{-z} \wedge \mathrm{y_r} \geq \mathrm{y} > \mathrm{y_r}\text{-r} \wedge 0 \leq \mathrm{z} < \mathrm{r}\}$
$U_{\mathrm{x3}} = \{(\mathrm{x,y,z}) \in U \mid \mathrm{y} \leq \mathrm{x} < \mathrm{x_r}\text{-y} \wedge \mathrm{z_r}\text{-z} < \mathrm{x} \leq \mathrm{z} \wedge 0 \leq \mathrm{y} < \mathrm{r} \wedge \mathrm{z_r} \geq \mathrm{z} > \mathrm{z_r}\text{-r}\}$
$U_{\mathrm{x4}} = \{(\mathrm{x,y,z}) \in U \mid \mathrm{y_r}\text{-y} < \mathrm{x} \leq \mathrm{y} \wedge \mathrm{z_r}\text{-z} < \mathrm{x} \leq \mathrm{z} \wedge \mathrm{y_r} \geq \mathrm{y} > \mathrm{y_r}\text{-r} \wedge \mathrm{z_r} \geq \mathrm{z} > \mathrm{z_r}\text{-r}\}$
$U_{\mathrm{y1}} = \{(\mathrm{x,y,z}) \in U \mid \mathrm{r} \leq \mathrm{y} < \mathrm{y_r}\text{-z} \wedge \mathrm{r} \leq \mathrm{y} \leq \mathrm{y_r x} \wedge 0 \leq \mathrm{x} < \mathrm{r} \wedge 0 \leq \mathrm{z} < \mathrm{r}\}$
$U_{\mathrm{y2}} = \{(\mathrm{x,y,z}) \in U \mid \mathrm{z} \leq \mathrm{y} < \mathrm{y_r}\text{-z} \wedge \mathrm{x_r}\text{-x} \leq \mathrm{y} < \mathrm{x} \wedge \mathrm{x_r} \geq \mathrm{x} > \mathrm{x_r}\text{-r} \wedge 0 \leq \mathrm{z} < \mathrm{r}\}$
$U_{\mathrm{y3}} = \{(\mathrm{x,y,z}) \in U \mid \mathrm{z_r}\text{-z} < \mathrm{y} \leq \mathrm{z} \wedge \mathrm{x} < \mathrm{y} \leq \mathrm{y_r}\text{-x} \wedge 0 \leq \mathrm{x} < \mathrm{r} \wedge \mathrm{z_r} \geq \mathrm{z} > \mathrm{z_r}\text{-r}\}$
$U_{\mathrm{y4}} = \{(\mathrm{x,y,z}) \in U \mid \mathrm{z_r}\text{-z} \leq \mathrm{y} < \mathrm{z} \wedge \mathrm{x_r}\text{-x} < \mathrm{y} \leq \mathrm{x} \wedge \mathrm{x_r} \geq \mathrm{x} > \mathrm{x_r}\text{-r} \wedge \mathrm{z_r} \geq \mathrm{z} > \mathrm{z_r}\text{-r}\}$
$U_{\mathrm{z1}} = \{(\mathrm{x,y,z}) \in U \mid \mathrm{r} \leq \mathrm{z} \leq \mathrm{z_r}\text{-x} \wedge \mathrm{r} \leq \mathrm{z} \leq \mathrm{z_r}\text{-y} \wedge 0 \leq \mathrm{x} < \mathrm{r} \wedge 0 \leq \mathrm{y} < \mathrm{r}\}$
$U_{\mathrm{z2}} = \{(\mathrm{x,y,z}) \in U \mid \mathrm{x} < \mathrm{z} \leq \mathrm{z_r}\text{-x} \wedge \mathrm{y_r}\text{-y} \leq \mathrm{z} < \mathrm{y} \wedge 0 \leq \mathrm{x} < \mathrm{r} \wedge \mathrm{y_r} \geq \mathrm{y} > \mathrm{y_r}\text{-r}\}$
$U_{\mathrm{z3}} = \{(\mathrm{x,y,z}) \in U \mid \mathrm{x_r}\text{-x} \leq \mathrm{z} < \mathrm{x} \wedge \mathrm{y} < \mathrm{z} \leq \mathrm{z_r}\text{-y} \wedge \mathrm{x_r} \geq \mathrm{x} > \mathrm{x_r}\text{-r} \wedge 0 \leq \mathrm{y} < \mathrm{r}\}$
$U_{\mathrm{z4}} = \{(\mathrm{x,y,z}) \in U \mid \mathrm{x_r}\text{-x} \leq \mathrm{z} < \mathrm{x} \wedge \mathrm{y_r}\text{-y} \leq \mathrm{z} < \mathrm{y} \wedge \mathrm{x_r} \geq \mathrm{x} > \mathrm{x_r}\text{-r} \wedge \mathrm{y_r} \geq \mathrm{y} > \mathrm{y_r}\text{-r}\}$
$U_{\mathrm{in}} = \{(\mathrm{x,y,z}) \in U \mid 0 \leq \mathrm{x} < \mathrm{r} \wedge 0 \leq \mathrm{y} < \mathrm{r} \wedge 0 \leq \mathrm{z} < \mathrm{r}\}$
$U_{\mathrm{out}} = \{(\mathrm{x,y,z}) \in U \mid \mathrm{x_r}\text{-r} \leq \mathrm{x} < \mathrm{x_r} \wedge \mathrm{y_r}\text{-r} \leq \mathrm{y} < \mathrm{y_r} \wedge \mathrm{z_r}\text{-r} \leq \mathrm{z} < \mathrm{z_r}\}$.

The BBB is represented by a subset $U_{\mathrm{BBB}} \subset U$, such that $U_{\mathrm{BBB}} = \partial\, U_{\mathrm{pl}} \backslash \partial\, U$. This denotes the border between the blood plasma and the brain ECF, located at distance r from the edges of the 3D brain unit.
The brain ECF is represented by a subset $U_{\mathrm{ECF}} \subset U$, such that $U_{\mathrm{ECF}} = U \backslash (U_{\mathrm{pl}} \cup U_{\mathrm{BBB}})$.
Within U we define the following quantities describing drug concentration:

C_{pl} (x,y,z,t): U_{pl} x $\mathbb{R}^+ \to \mathbb{R}^+$,
C_{ECF} (x,y,z,t): U_{ECF}x $\mathbb{R}^+ \to \mathbb{R}^+$,
B_1 (x,y,z,t): U_{ECF}x $\mathbb{R}^+ \to \mathbb{R}^+$,
B_2 (x,y,z,t): U_{ECF} x $\mathbb{R}^+ \to \mathbb{R}^+$.
Here, C_{pl} is the concentration of unbound drug in the blood plasma, C_{ECF} is the concentration of unbound drug in the brain ECF, B_1 is the concentration of drug in the brain ECF bound to specific binding sites and B_2 is the concentration of drug in the brain ECF bound to non-specific binding sites.

2.2 Description of drug distribution in U_{pl}

Based on assumption 1(i), we define the concentration of (unbound) drug within U_{in} by including parameters related to oral administration [30]:

$$C_{\mathrm{pl}} = \frac{F k_{\mathrm{a}} Dose}{V_{\mathrm{d}}(k_{\mathrm{a}} - k_{\mathrm{e}})}(e^{-k_{\mathrm{e}}\mathrm{t}} - e^{-k_{\mathrm{a}}\mathrm{t}}) \text{ for } C_{\mathrm{pl}} \in U_{\mathrm{in}} \tag{1}$$

, where F is the bioavailability of the drug, k_{a} the absorption rate constant of the drug, k_{e} the elimination rate constant of the drug, $Dose$ the molar amount of orally administered drug, and V_{d} the distribution volume, which relates the total amount of drug in the body to the drug concentration in the blood plasma. We focus on oral administration but can also study other choices.
Additionally, based on assumptions 1(iv) and 1(v), we define:

$$\frac{\mathrm{d}C_{\mathrm{pl}}}{\mathrm{dt}} = -v_{\mathrm{blood}}\frac{\partial C_{\mathrm{pl}}}{\partial \mathrm{x}} \text{ for } C_{\mathrm{pl}} \in U_{\mathrm{xi}}, \text{ for i=1,..,4,} \tag{2}$$

$$\frac{\mathrm{d}C_{\mathrm{pl}}}{\mathrm{dt}} = -v_{\mathrm{blood}}\frac{\partial C_{\mathrm{pl}}}{\partial \mathrm{y}} \text{for } C_{\mathrm{pl}} \in U_{\mathrm{yi}}, \text{ for i=1,..,4,} \tag{3}$$

$$\frac{\mathrm{d}C_{\mathrm{pl}}}{\mathrm{dt}} = -v_{\mathrm{blood}}\frac{\partial C_{\mathrm{pl}}}{\partial \mathrm{z}} \text{ for } C_{\mathrm{pl}} \in U_{\mathrm{zi}}, \text{ for i=1,..,4,} \tag{4}$$

, with v_{blood} the blood flow velocity within the brain capillaries and where the initial condition is given by

$$C_{\mathrm{pl}}(\mathrm{x}, \mathrm{y}, \mathrm{z}, \mathrm{t} = 0) = 0. \tag{5}$$

2.3 Description of drug distribution in U_{ECF}

Based on assumptions 2, we describe the distribution of unbound and bound drug within U_{ECF} with the following system of equations:

$$\begin{aligned}
\frac{\partial C_{\mathrm{ECF}}}{\partial t} &= \frac{D}{\lambda^2}\nabla^2 C_{\mathrm{ECF}} - v_{\mathrm{ECF}}\frac{\partial C_{\mathrm{ECF}}}{\partial \mathrm{x}} - k_{1\mathrm{on}} C_{\mathrm{ECF}}(B_1^{\max} - B_1) + k_{1\mathrm{off}} B_1 \\
&\quad - k_{2\mathrm{on}} C_{ECF}(B_2^{\max} - B_2) + k_{2\mathrm{off}} B_2 \\
\frac{\partial B_1}{\partial t} &= k_{1\mathrm{on}} C_{\mathrm{ECF}}(B_1^{\max} - B_1) - k_{1\mathrm{off}} B_1 \\
\frac{\partial B_2}{\partial t} &= k_{2\mathrm{on}} C_{\mathrm{ECF}}(B_2^{\max} - B_2) - k_{2\mathrm{off}} B_2.
\end{aligned} \tag{6}$$

with initial conditions

$$C_{\mathrm{ECF}}(\mathrm{x},\mathrm{y},\mathrm{z},\mathrm{t}=0)=0 \tag{7}$$

,

$$B_{\mathrm{i}}(\mathrm{x},\mathrm{y},\mathrm{z},\mathrm{t}=0)=0,\mathrm{i}=1,2 \tag{8}$$

, where D is the diffusion coefficient in a free medium, λ the tortuosity, v_{ECF} the (x-directed) brain ECF bulk flow, ${B_1}^{\max}$,the total concentration of specific binding sites within the brain ECF, $k_{1\mathrm{on}}$ the association rate constant for specific binding, $k_{1\mathrm{off}}$ the dissociation rate constant for specific binding, ${B_2}^{\max}$ the total concentration of non-specific binding sites within the brain ECF, $k_{2\mathrm{on}}$the association rate constant for non-specific binding and $k_{2\mathrm{off}}$ the dissociation rate constant for non-specific binding.

2.4 Boundary conditions

We formulate boundary conditions that describe the change in concentration of drug at the boundary between the blood-plasma-domain (U_{ok}) and the brain-ECF-domain (U_{ECF}), hence at U_{BB} as well as at the boundaries of the 3D brain unit ($U_{\mathrm{pl}}\cap\partial\ U$, $U_{\mathrm{ECF}}\cap\partial U$).

2.4.1 Drug exchange between U_{pl} and U_{ECF}

We describe diffusive transport by the difference in drug concentrations in C_{ECF} and C_{pl}, multiplied by the BBB permeability, P. In addition, we model active transport into and out of the brain ECF with Michaelis-Menten kinetics, similar to the approach of [6]. In total, this leads to:

$$\begin{aligned}&\mathrm{f}(\mathrm{u},\mathrm{v})=P(\mathrm{u}-\mathrm{v})+\frac{T_{\mathrm{m-in}}}{SA_{\mathrm{BBB}}(K_{\mathrm{m-in}}+\mathrm{u})}\mathrm{u}-\frac{T_{\mathrm{m-out}}}{SA_{\mathrm{BBB}}(K_{\mathrm{m-out}}+\mathrm{v})}\mathrm{v},\\&\text{with } P=P_{\mathrm{trans}}f_{\mathrm{trans}}+P_{\mathrm{para}}f_{\mathrm{para}},\\&\text{with } P_{\mathrm{para}}=\frac{D_{\mathrm{para}}}{W_{\mathrm{PCS}}}\end{aligned} \tag{9}$$

, with u = C_{pl}, v= C_{ECF}, P_{trans} being the permeability through the brain endothelial cells, f_{trans} the fraction of the area occupied by the brain endothelial cells, $D_{\mathrm{para}}$the diffusivity of a drug across the paracellular space, W_{PCS} the width of the paracellular space, f_{para} the fraction of area occupied by the paracellular space, $T_{\mathrm{m\text{-}in}}$ the maximum rate of drug active influx, $T_{\mathrm{m\text{-}out}}$ the maximum rate of drug active efflux, $K_{\mathrm{m\text{-}in}}$ the concentration of drug at which half of $T_{\mathrm{m\text{-}in}}$ is reached, $K_{\mathrm{m\text{-}out}}$ the concentration of drug at which half of $T_{\mathrm{m\text{-}out}}$ is reached and SA_{BBB} the surface area of the BBB. Based hereon, we describe the loss or gain of unbound drug in the brain ECF due to BBB transport with the following boundary conditions (only those for the x direction are given, the ones for the y and z directions are similar):

$$\begin{aligned}-D^*\frac{\partial C_{\mathrm{ECF}}}{\partial \mathrm{x}}&=\mathrm{f}(\mathrm{C_{pl}},\mathrm{C_{ECF}}),\ \text{for (x,y,z)}\in U_{\mathrm{BBB}}\ \text{, at x=r,}\\D^*\frac{\partial C_{\mathrm{ECF}}}{\partial \mathrm{x}}&=\mathrm{f}(\mathrm{C_{pl}},\mathrm{C_{ECF}}),\ \text{for (x,y,z)}\in U_{\mathrm{BBB}}\ \text{at x=}x_{\mathrm{r}}\text{-r.}\end{aligned} \tag{10}$$

For the blood-plasma-domain, U_{pl}, we use the reverse of (12) to describe drug transport across the BBB in the brain capillaries with the following boundary conditions:

$$\begin{aligned}D^*\frac{\partial C_{\mathrm{pl}}}{\partial \mathrm{x}}&=\mathrm{f}(\mathrm{C_{pl}},\mathrm{C_{ECF}}),\text{for (x,y,z)}\in U_{\mathrm{BBB}},\text{ at x=r,}\\D^*\frac{\partial C_{\mathrm{pl}}}{\partial \mathrm{x}}&=-\mathrm{f}(\mathrm{C_{pl}},\mathrm{C_{ECF}}),\text{for (x,y,z)}\in U_{\mathrm{BBB}},\text{ at x=}x_{\mathrm{r}}\text{-r.}\end{aligned} \tag{11}$$

2.4.2 Drug exchange at the faces of the 3D brain unit

We use additional boundary conditions to describe the drug concentrations at the sides of the domain. Since we assume that there is no diffusion in the blood plasma (see assumption 1(v)), we use the following boundary conditions:

$$\frac{\partial C_{\mathrm{pl}}}{\partial \mathrm{x}} = 0 \tag{12}$$

, for (x,y,z) $\in$ $_{\mathrm{pl}}\backslash\ U_{\mathrm{out}} \cap \partial\ U$, for x=0 and x=$\mathrm{x_r}$,

$$\frac{\partial C_{\mathrm{pl}}}{\partial \mathrm{y}} = 0 \tag{13}$$

, for (x,y,z) $\in\ U_{\mathrm{pl}}\ \backslash\ U_{\mathrm{out}} \cap \partial\ U$, for y=0 and y=$\mathrm{y_r}$,

$$\frac{\partial C_{\mathrm{pl}}}{\partial \mathrm{z}} = 0 \tag{14}$$

, , for (x,y,z) $\in$ $_{\mathrm{pl}}\backslash\ U_{\mathrm{out}} \cap \partial\ U$, for z=0 and z=$\mathrm{z_r}$.
In addition, we define:

$$C_{\mathrm{pl}} = 0 \tag{15}$$

, for (x,y,z) $\in\ U_{\mathrm{out}} \cap \partial\ U$.
We formulate the condition at the boundaries of the 3D brain unit as follows:

$$\frac{\partial C_{\mathrm{ECF}}}{\partial x} = 0 \tag{16}$$

, for $U_{\mathrm{ECF}} \cap \partial\ U$.

2.5 Model parameter values and units

The dimensions of the 3D brain unit are based on the properties of the rat brain. The model is suitable for data from human or other species as well, but we have chosen for the rat as for this species most data is available. The distance between the brain capillaries in the rat brain is on average 50 μm, while the brain capillaries have a radius of about 2.5 μm [31–34]. Therefore, we set the radius of the brain capillaries, r, to 2.5 μm and the dimensions of the 3D brain unit in the x, y and z directions, x_{r}, y_{r} and z_{r} respectively, to 55 μm.
In our model, we use Eq (2)-(6) to describe drug concentration within the blood plasma, with boundary conditions described in Eq (13)-(17). We describe the concentration of drug within the brain ECF with Eq (7)-(9) with boundary conditions described in (11),(12) and (18). The range of values we use for the parameters in the model as well as their units are given in Table 1 below. This range is based on values found in the literature (from experimental studies), which we also give in the table. The literature does not provide values on the kinetic parameters related to non-specific binding kinetics ($B_2{}^{\mathrm{max}}$, $k_{2\mathrm{on}}$ and $k_{2\mathrm{off}}$). Therefore, we base the choices of these values on earlier articles that assume that drug binding to specific binding sites is stronger than to non-specific binding sites, while non-specific binding sites are more abundant [29, 35, 36].

3 Model results

We study the distribution of a drug within the 3D brain unit by plotting its concentration-time profiles within the brain ECF (brain ECF PK). In addition, we

Table 1. 3D brain unit model parameters and their units, for rat brain. The physiological range of values of the parameters is given. These are based on references from the literature.

Parameter	Unit	Range of values	Ref.
F, bioavailability	-	0-1	[30]
$Dose$	μmol	10^{-1}-10^{2}	
V, distribution volume	L	0.05-5	[38]
k_{a}, absorption rate constant	s^{-1}	0-2·10^{-3}	[38]
			[20]
k_{e}, elimination rate constant	s^{-1}	5·10^{-5}-3·10^{-2}	[38]
			[20]
d_{cap}, intercapillary distance	m	2·10^{-5}-7·10^{-5}	[31]
			[39]
r, brain capillary radius	m	0.8-4.8·10^{-6}	[39]
			[34]
v_{blood}, brain capillary blood flow velocity	m s^{-1}	0.5-50·10^{-4}	e.g. [5]
$D^{*}=\frac{D}{\lambda^{2}}$, effective diffusion coefficient	m^2s^{-1}	10^{-11}-10^{-10}	[40]
			[41]
v_{ECF}, brain ECF bulk flow velocity	m s^{-1}	5·10^{-8}-5·10^{-6}	[42]
			[43]
P, 3D passive BBB permeability[1]	m s^{-1}	10^{-10}-10^{-5}	[44][2]
$T_{\mathrm{m\text{-}in}}$, maximal active influx rate	μmol s^{-1}	10^{-8}-10^{-5}	[45]
$K_{\mathrm{m\text{-}in}}$, concentration needed to reach half of $T_{\mathrm{m\text{-}in}}$	μmol L^{-1}	10^{1}-10^{4}	[46]
$T_{\mathrm{m\text{-}out}}$, maximal active efflux rate	μmol s^{-1}	10^{-8}-10^{-5}	[45]
$K_{\mathrm{m\text{-}out}}$, concentration needed to reach half of $T_{\mathrm{m\text{-}out}}$	μmol L^{-1}	10^{1}-10^{4}	[46]
SA_{BBB} surface area of the BBB[6]	m^2	1.25·10^{-10}	
${B_1}^{\mathrm{max}}$, total concentration specific binding sites	μmol L^{-1}	1·10^{-3}-5·10^{-1}	[16][3]
$k_{1\mathrm{on}}$, specific association constant	(μmol $L^{-1}s$)$^{-1}$	10^{-4}-10^{2}	[16][4]
$k_{1\mathrm{off}}$, specific dissociation constant	s^{-1}	10^{-6}-10^{1}	[16][4]
${B_1}^{\mathrm{max}}$, total non-specific binding sites	μmol L^{-1}	1·10^{1}-5·10^{3}	[29]
$k_{2\mathrm{on}}$, non-specific association constant	(μmol $L^{-1}s$)$^{-1}$	10^{-6}-10^{1}	[29]
$k_{2\mathrm{off}}$, non-specific dissociation constant	s^{-1}	10^{-4}-10^{3}	[29]

[1] This value is the apparent (experimentally measured) overall passive permeability [44].

[2] [47–50]

[3] [51–56]

[4] http://www.k4dd.eu and [57]

[5] [58–62], [63]

[6] This is the surface area of the BBB that separates one side of a brain capillary within the 3D brain unit from the brain ECF.

Table 2. 3D brain unit model default parameter values and their units. The values are for a hypothetical drug and are all within the physiological ranges given in Table 1.

Parameter	Unit	Value
F	-	1
$Dose$	μmol	0.5
k_{a}	s^{-1}	$2{\cdot}10^{-4}$
k_{e}	s^{-1}	$5{\cdot}10^{-5}$
V	L	0.2
d_{cap}	m	$5{\cdot}10^{-5}$
r	m	$2.5{\cdot}10^{-6}$
v_{blood}	m s^{-1}	$5{\cdot}10^{-4}$
D^*	$\mathrm{m}^2\mathrm{s}^{-1}$	$0.5{\cdot}10^{-10}$
v_{ECF}	m s^{-1}	$0.5{\cdot}10^{-6}$
P	m s^{-1}	$0.1{\cdot}10^{-7}$
$T_{\mathrm{m\text{-}in}}$	μmol s^{-1}	$0{\cdot}10^{-7}$
$T_{\mathrm{m\text{-}out}}$	μmol s^{-1}	$0{\cdot}10^{-7}$
$K_{\mathrm{m\text{-}in}}$	μmol L^{-1}	$1{\cdot}10^{2}$
$K_{\mathrm{m\text{-}out}}$	μmol L^{-1}	$1{\cdot}10^{2}$
SA_{BBB}	m^2	$1{\cdot}10^{-10}$
${B_1}^{\mathrm{max}}$	μmol L^{-1}	$5{\cdot}10^{-2}$
$k_{1\mathrm{on}}$	$(\mu\mathrm{mol}\ \mathrm{L}^{-1}\mathrm{s})^{-1}$	1
$k_{1\mathrm{off}}$	s^{-1}	$1{\cdot}1^{-2}$
${B_1}^{\mathrm{max}}$	μmol L^{-1}	$5{\cdot}10^{1}$
$k_{2\mathrm{on}}$	$(\mu\mathrm{mol}\ \mathrm{L}^{-1}\mathrm{s})^{-1}$	$1{\cdot}10^{-2}$
$k_{2\mathrm{off}}$	s^{-1}	1

study the distribution of the drug within the 3D brain unit. We first nondimensionalise the system of equations and boundary conditions by scaling all variables by a characteristic scale, see S1 Appendix for details. Next, in order to perform simulations, we discretise the nondimensionalised system spatially, using a well-established numerical procedure based on finite element approximations [37]. We present the results using the parameters with dimensions. The output of the simulations are the concentrations of free, specifically bound and non-specifically bound drug, given in μmol L^{-1} over time (s). The model can easily be used to study a specific drug by choosing the parameter values that are specific for this drug, provided that parameter values for this drug are known. In the present study, however, we choose to study generic parameter values that are in the middle of the physiological ranges given in Table 1 . This allows us to perform a sensitivity analysis and study the effect of parameter values at both extremes of the physiological range on the behaviour of the model. We use, unless otherwise indicated, the parameter values that are given in Table 2. In the following sections, we show the impact of the brain capillary blood flow velocity (v_{blood}) in the absence of active transport (section 3.1), the impact of active transport (section 3.2) and the impact of v_{blood} and active transport combined (section 3.3) on blood plasma and brain ECF PK and brain ECF drug distribution. We give the concentration-time profiles of unbound drug, specifically bound drug and non-specifically bound drug in the middle of U_{ECF}, where (x,y,z)=($\frac{\mathrm{x_r}}{2}$, $\frac{\mathrm{y_r}}{2}$, $\frac{\mathrm{z_r}}{2}$) as well as those of unbound drug in the blood plasma in the middle of U_{x1}, where (x,y,z)=($\frac{\mathrm{x_r}}{2}$,$\frac{r}{2}$, $\frac{r}{2}$), on a log-scale versus time. Drug distribution profiles are given for cross-sections of the entire (x,y,z)-domain of the 3D brain unit for various times.

Fig 3. The effect of the brain capillary blood flow velocity, v_{blood} (m s^{-1}), on the log PK of C_{pl} (red) and C_{ECF} (top), B_1 (middle) and B_2 (bottom) for a default (P=0.1·10^{-7}m s^{-1}) (left) and a high (P=100·10^{-7}m s^{-1}) (right) value of P. Values of v_{blood} are set at 0.05·10^{-4} m s^{-1}, 0.5·10^{-4} m s^{-1}, 5·10^{-4} m s^{-1}, 50·10^{-4} m s^{-1} and 500·10^{-4} m s^{-1}, as is depicted by different colours, where drug concentrations for the default value of v_{blood} (v_{blood}=5·10^{-4} m s^{-1}) are shown in blue. All other parameters are as in Table 2. The insets in each sub-figure show the PK for a shorter time.

3.1 The effect of the brain capillary blood flow velocity on brain ECF PK within the 3D brain unit

The impact of the brain capillary blood flow velocity, v_{blood}, on brain ECF PK within the 3D brain unit is evaluated. Parameters are as in Table 2 and we thus assume that there is no active transport, i.e. $T_{\text{m-in}}$=0 and $T_{\text{m-out}}$=0. Here, we focus on the effect of v_{blood} on brain ECF PK in the middle of the 3D brain unit. We show the concentration-time profiles of unbound, specifically bound and non-specifically bound drug (C_{ECF}, B_1 and B_2, respectively) within the 3D brain unit on a larger time-scale, for several values of v_{blood}. We do so for the default value of the passive permeability P (P=0.1·10^{-7} m s^{-1}), in Fig 3 (left), as well as for a high value of P (P=100·10^{-7} m s^{-1}), in Fig 3 (right). The lowest value of v_{blood} is outside the known physiological ranges (see Table 1), but we choose it as v_{blood} is predicted to mostly impact drug concentrations in the brain when P is much higher than v_{blood} [64, 65]. The total passive permeability, P, includes both transcellular and paracellular permeability. The paracellular space may increase due to disruption of the tight junctions in certain disease conditions, thereby allowing larger molecules to pass through and increasing paracellular transport [66, 67]. We can tune our model and separate between transcellular and paracellular transport, as we do in S2 Appendix. In the current section we proceed with the total passive BBB permeability.

Fig 3 shows that v_{blood} does not impact long-time behaviour of C_{ECF}, B_1 and B_2. The insets in Fig 3 demonstrate that v_{blood} impacts short-time (t=0-100 s) behaviour only when it has extremely low values ($v_{\text{blood}}\leq$0.5·10^{-4} m s^{-1}), as depicted in the insets of Fig 3 by the yellow and purple lines, respectively. The impact of v_{blood} on C_{ECF}, B_1 and B_2 is independent of the values of P (compare the left and right insets of Fig 3). The effects of P on drug concentrations within the brain ECF are similar to those found with our proof-of-concept 2D model [29]: for a high value of P, the attained values of C_{ECF} and B_2 are higher and follow C_{pl}, while their decay is faster than for a low value of P. In addition, the $\geq$90% maximum value of B_1, i.e. values of B_1 that are more than 90% of the maximum value attained during the simulation ($B_1 \geq$90% max(B_1)), is attained shorter for a high value of P than for a low value of P.

From the results shown in Fig 3 we conclude that the effects of v_{blood} on brain ECF PK are minimal. According to the Renkin-Crone equation [64, 65], the brain capillary blood flow affects drug *influx*, depending on the permeability of the BBB. This is also demonstrated by our model, and we show that v_{blood} affects drug influx across the BBB in S3 Appendix.

The plots in Fig 4a show the changes in concentration of drug within the blood plasma over a short time-range (t=5 to t=25). There, C_{pl} is plotted along the capillaries starting at U_{in} (where drug enters the unit) to U_{out} (where drug exits the unit). We measure the distance from U_{in}, where the total distance between these points is 150 μm. Drug can be transported along several pathways, but in Fig 4a the values of C_{pl} are given along the pathway indicated in Fig 4b. When v_{blood}=0.5 (left), there are clear differences between C_{pl} in U_{in} (Distance=0) and C_{pl} in the opposite corner (Distance=150) at the time-points shown. However, as C_{pl} increases over time, the

Fig 4. Changes in C_{pl} and C_{ECF} due to the effect of v_{blood}. While v_{blood} is varied from $0.05{\cdot}10^{-4}$ m s^{-1} to $50{\cdot}10^{-4}$ m s^{-1}, all other parameter values are as in Table 2. a) The pathway from U_{in} to U_{out} along which C_{pl} is plotted. b) C_{pl} is plotted against time (timepoints from 5 to 25) along the distance shown in (a). c) Distribution profiles of C_{pl} (red) and C_{ECF} (blue) of the 3D brain unit at t=5. Darker shades of red and blue correspond to higher values of C_{pl} and C_{ECF}, respectively.

Fig 5. The effect of active influx on the log concentration-time profiles of drug in the brain ECF, relative to those in the blood plasma. Top: unbound drug in the brain ECF (C_{ECF}) compared to unbound drug in the blood plasma (C_{pl}, red curve). Middle: drug bound to its target sites (B_1). Bottom: drug bound to non-specific binding sites (B_2). The value of $T_{\text{m-in}}$ is changed from 0 to $100{\cdot}10^{-7}$ μmol s^{-1}. The rest of the parameters are as in Table 2.

differences in C_{pl} become small relative to the value of C_{pl}. Fig 4c shows the distribution profiles of unbound drug within the 3D brain unit at t=5 for different values of v_{blood}. There, darker shades of red and blue correspond to higher concentrations of unbound drug in the blood plasma and the brain ECF, respectively. When v_{blood}=$0.5{\cdot}10^{-4}$ m s^{-1}, the transport time of drug between U_{in} and the opposite corner is higher than when v_{blood}=$5{\cdot}10^{-4}$ m s^{-1}. This is depicted in Fig 4c, where at t=5, drug concentrations within U_{pl} are equal for a high brain capillary blood flow velocity (v_{blood}=$50{\cdot}10^{-4}$ m s^{-1}), while local differences in C_{pl} still exist for a low value of v_{blood} (v_{blood}=$0.5{\cdot}10^{-4}$ m s^{-1}). The value of v_{blood} also affects local concentrations of C_{ECF}. For a low value of v_{blood} (v_{blood}=$0.5{\cdot}10^{-4}$ m s^{-1}), values of C_{ECF} at t=5 are overall low, but highest in the corners closest to U_{in}. For higher values of v_{blood} (v_{blood}=$5{\cdot}10^{-4}$ m s^{-1} and v_{blood}=$50{\cdot}10^{-4}$ m s^{-1}), C_{ECF} at t=5 is overall higher, but again highest in the corner close to U_{in}.

3.2 The effect of active transport on the drug concentrations within the brain ECF

Active transport kinetics are regulated by the maximal transport rate (T_{m}) and the concentration of drug needed to reach half of the maximal transport rate (K_{m}), see section 2.4.1. We first focus on active influx, such that $T_{\text{m-out}}$=0. We vary $T_{\text{m-in}}$, which denotes the maximal rate of active transporters moving drug from the blood plasma *into* the brain ECF. Fig 5 shows the effects of increasing values of $T_{\text{m-in}}$ (starting at $T_{\text{m-in}}$=0, i.e. no active influx) on C_{ECF} (top), B_1 (middle) and B_2 (bottom). Fig 5 (top) reveals that an increased value of $T_{\text{m-in}}$ correlates with increased concentrations of C_{ECF}. The time to the peak of C_{ECF} is not affected by the value of $T_{\text{m-in}}$. Fig 5 (middle) shows that $T_{\text{m-in}}$ does affect the time during which the specific binding sites are saturated. We find that 90% max(B_1) is attained longer for a higher $T_{\text{m-in}}$. Fig 5 (bottom) shows that higher values of $T_{\text{m-in}}$ correlate with higher values of B_2 and thus a greater occupancy of non-specific binding sites. The non-specific binding sites within the brain ECF become saturated with drug when $T_{\text{m-in}}$ is sufficiently high ($T_{\text{m-in}}$=$100{\cdot}10^{-7}$ μmol s^{-1}). To evaluate the effect of active efflux on drug concentrations within the brain ECF, we repeat our simulations with T_{m} directed outward, i.e. with $T_{\text{m-out}}$=0-$100{\cdot}10^{-7}$ μmol s^{-1} and $T_{\text{m-in}}$=0. Fig 6 (top) shows that C_{ECF} decreases faster for higher values of $T_{\text{m-out}}$, corresponding to more active efflux. Fig 6 (middle) reveals that $T_{\text{m-out}}$ affects the time during which specific binding sites are saturated: the time at which B_1 attains 90% max(B_1) is smaller for a high value of $T_{\text{m-out}}$. For sufficiently high values of $T_{\text{m-out}}$, the binding sites do not become saturated. Fig 6 (bottom) shows that B_2 is similarly affected by active efflux as C_{ECF}.

Fig 6. The effect of active efflux on the log concentration-time profiles of drug in the brain ECF, relative to those in the blood plasma. Top: unbound drug in the brain ECF (C_{ECF}) and unbound drug in the blood plasma (C_{pl}, red curve). Middle: drug bound to its target sites (B_1). Bottom: drug bound to non-specific binding sites (B_2). The value of $T_{\mathrm{m\text{-}out}}$ is changed from 0 to $100{\cdot}10^{-7}$ μmol s^{-1}. The rest of the parameters are as in Table 2.

Fig 7. The log concentration-time profiles of unbound drug in brain ECF (C_{ECF}) with 1000x increased permeability P (left to right, $0.1{\cdot}10^{-7}$ m s^{-1} to $100{\cdot}10^{-7}$ m s^{-1}) or 10x decreased flow v_{ECF} (top to bottom, $5{\cdot}10^{-4}$m s^{-1} to $0.5{\cdot}10^{-4}$ m s^{-1}) in the presence of active influx compared to the concentration of unbound drug in the blood plasma (C_{pl}, red curve). The value of of $T_{\mathrm{m\text{-}in}}$ is changed from 0 to $100{\cdot}10^{-7}$ μmol s^{-1}, as depicted by various colours. The rest of the parameters are as in Table 2.

3.3 The effect of the brain capillary blood flow velocity in the presence of active transport

In section 3.1 we have shown that both the passive BBB permeability, P, and the brain capillary blood flow velocity, v_{blood}, affect dug brain ECF PK in the absence of active transport. Here, we study how P and v_{blood} combined with active transport affect drug PK within the brain ECF. Fig 7 shows the log plot of C_{ECF} for $v_{\mathrm{blood}}{=}5{\cdot}10^{-4}$ m s^{-1} (top) and $v_{\mathrm{blood}}{=}0.5{\cdot}10^{-4}$ m s^{-1} (bottom) and for $P{=}0.1{\cdot}10^{-7}$ m s^{-1} (left) and $P{=}100{\cdot}10^{-7}$ m s^{-1} (right) in the presence of active influx, i.e. for various values of $T_{\mathrm{m\text{-}in}}$ ($T_{\mathrm{m\text{-}out}}{=}0$). Note that the vertical scale is the same in all plots. Fig 7 shows how P and v_{blood} affect the impact of $T_{\mathrm{m\text{-}in}}$ on brain ECF PK. A smaller value of v_{blood} only slightly reduces C_{ECF} when $T_{\mathrm{m\text{-}in}}$ is sufficiently high ($T_{\mathrm{m\text{-}in}}{\geq}10{\cdot}10^{-7}$ μmol s^{-1}), see Fig 7, left. An increase in P does reduce the impact of $T_{\mathrm{m\text{-}in}}$ on C_{ECF} substantially (Fig 7, right). When the BBB is very permeable, active influx needs to be fast to have any effect, as drug can easily pass the BBB to flow back into the blood plasma. As shown in Fig 7, right, in the presence of a high value of P, $T_{\mathrm{m\text{-}in}}$ only (slightly) affects C_{ECF} when it is $10{\cdot}10^{-7}$ μmol s^{-1} or higher.

Fig 8 shows the log profiles of C_{ECF} for $v_{\mathrm{blood}}{=}5{\cdot}10^{-4}$ m s^{-1} (top) and $v_{\mathrm{blood}}{=}0.5{\cdot}10^{-4}$ m s^{-1} (bottom) and for $P{=}0.1{\cdot}10^{-7}$ m s^{-1} (left) and $P{=}100{\cdot}10^{-7}$ m s^{-1} (right) in the presence of active efflux, i.e. for various values of $T_{\mathrm{m\text{-}out}}$ ($T_{\mathrm{m\text{-}in}}$ =0). Fig 8 reveals that v_{blood} does not affect the impact of $T_{\mathrm{m\text{-}out}}$ on C_{ECF}. This is expected, as v_{blood} mainly affects C_{pl}, while active efflux depends on C_{ECF}. The passive permeability P does affect the impact of $T_{\mathrm{m\text{-}out}}$ on C_{ECF}. If P is high, drug can easily flow across the BBB back into the brain ECF, following the concentration gradient between the blood plasma and the brain ECF, thereby countering the effect of $T_{\mathrm{m\text{-}out}}$. Fig 8 (top right) shows that for a high P, C_{ECF} is only affected by $T_{\mathrm{m\text{-}out}}$ when its value is higher than $10{\cdot}10^{-7}$ μmol s^{-1}. The values of C_{ECF} in the presence of active efflux and a high passive BBB permeability, P, are unaffected by v_{blood} (Fig 8, right).

Next, we study how the drug distribution within the 3D brain unit is affected by v_{blood}, P, $T_{\mathrm{m\text{-}in}}$ and $T_{\mathrm{m\text{-}out}}$. Fig 9 shows cross-sections (for y=$\frac{1}{2}$y$_{\mathrm{r}}$ and z=0) of the 3D brain unit at t=5, in which the distribution of C_{pl} and C_{ECF} is plotted. The values of C_{pl} and C_{ECF} are represented by shades of red and blue, respectively, where darker shades

Fig 8. The PK on log-scale of unbound drug in brain ECF (C_{ECF}) with 1000x increased permeability P (left to right, $0.1{\cdot}10^{-7}$ m s^{-1} to $100{\cdot}10^{-7}$ m s^{-1}) and 10x decreased blood flow velocity v_{blood} (top to bottom, $5{\cdot}10^{-4}$ m s^{-1} to $0.5{\cdot}10^{-4}$ m s^{-1}) in the presence of active efflux compared to the concentration of unbound drug in the blood plasma (C_{pl}, red curve). The value of $T_{\mathrm{m\text{-}out}}$ is changed from 0 to $100{\cdot}10^{-7}$ μmol s^{-1}, as indicated by the different colours. The rest of the parameters are as in Table 2.

Fig 9. The distribution profiles at cross-sections (at y=$\frac{1}{2}$ y_r) of the 3D brain unit at t=5 of unbound drug in brain ECF with lower brain capillary blood flow velocity (v_{blood}=0.5·10^{-4} m s^{-1}, middle column), higher passive BBB permeability (P=100·10^{-7} m s^{-1}, right column), presence of active influx (middle row, $T_{m\text{-}in}$=1·10^{-7} μmol s^{-1}) and presence of active efflux (bottom row, $T_{m\text{-}out}$=1·10^{-7} μmol s^{-1}) at t=5. Parameters are as in Table 2.

Fig 10. Values of C_{ECF} (10^{-3} μmol L^{-1}) at several locations within the brain unit for different values of P and v_{blood} at t=500. a) Locations within the 3D brain unit. Corner 1: (x,y,z)=(r,r,r), Corner 2: (x,y,z)=(x_r-r,y_r-r,z_r-r), Edge: (x,y,z)= (0, $\frac{y_r}{2}$, $\frac{z_r}{2}$), Middle: (x,y,z)= ($\frac{x_r}{2}$, $\frac{y_r}{2}$, $\frac{z_r}{2}$). b) Values of C_{ECF} are shown for a low ((P=0.01·10^{-8} m s^{-1}) , default (P=0.1·10^{-8} m s^{-1}) and high (P=1·10^{-8} m s^{-1}) value of P in the top, middle and bottom table, respectively. Within each table, concentrations are given for several values of v_{blood} (v_{blood}=0.5·10^{-4} m s^{-1}, v_{blood}=5·10^{-4} m s^{-1} and v_{blood}=50·10^{-4} m s^{-1}, left to right), $T_{m\text{-}in}$ ($T_{m\text{-}in}$=0, $T_{m\text{-}in}$=1·10^{-7} μmol s^{-1}, $T_{m\text{-}in}$=10·10^{-7} μmol s^{-1} and $T_{m\text{-}in}$=100·10^{-7} μmol s^{-1}) and $T_{m\text{-}out}$ ($T_{m\text{-}out}$=0, $T_{m\text{-}out}$=1·10^{-7} μmol s^{-1}, $T_{m\text{-}out}$=10·10^{-7} μmol s^{-1} and $T_{m\text{-}out}$=100·10^{-7} μmol s^{-1}) at different locations. When $T_{m\text{-}in}$ is changed, $T_{m\text{-}out}$=0 and vice versa. c) Colour legend. In each table, colours are relative to the value of C_{ECF} in the middle of the unit in the absence of active transport for v_{blood}=5·10^{-4} m s^{-1}, of which the colour is denoted by "Default". The intensity of green corresponds to the extent of increase, and the intensity of red corresponds to the extent of decrease of C_{ECF} compared to the default. Other parameters are as in Table 2.

indicate higher concentrations. In Fig 9a (left) we give a plot for a default P and v_{blood} (Fig 9a, left). Then, we decrease v_{blood} (Fig 9a, middle) or increase P (Fig 9a, right). For a lower v_{blood}, relative differences of C_{pl} over space increase (Fig 9a, middle). Additionally, due to the decrease in C_{pl}, local differences in C_{ECF} become more apparent. A larger value of P results in an increased exchange of drug between the blood plasma and the brain ECF, such that C_{ECF} becomes higher (Fig 9a, right). Fig 9b shows that the presence of active influx ($T_{m\text{-}in}$=1·10^{-7} μmol s^{-1}) increases C_{ECF}. As a consequence, local differences within U_{ECF} become relatively small. With a low value of v_{blood}, local differences in U_{pl} become apparent (Fig 9b, middle). Finally, Fig 9c shows that with active efflux, C_{ECF} becomes smaller than when no active efflux is present, except for when P is high and more pronounced.

Values of C_{ECF} are given in the table in Fig 10c in order to show the differences within the 3D brain unit more clearly. There, values of C_{ECF} are given for four different locations within the 3D brain unit for several values of v_{blood} and P and t=500. The table again (as in Fig 7, 8 and 9) shows that v_{blood} and P affect the impact of $T_{m\text{-}in}$ and $T_{m\text{-}out}$ on C_{ECF}. It provides additional information on the distribution of C_{ECF} within the 3D brain unit. In general, C_{ECF} is higher in the corners relative to the edge and middle within the 3D brain unit. The extent of these local concentration differences depends on the values of $T_{m\text{-}in}$ and $T_{m\text{-}out}$. The differences are largest when $T_{m\text{-}out}$=1·10^{-7} μmol s^{-1}, depicted in the lowest line of each sub-table. There, C_{ECF} in corner 2 is higher than in corner 1. In addition, in the presence of active influx, the values of C_{ECF} are lower in corner 2 than in corner 1. Again, the extent of this difference depends on the value of $T_{m\text{-}in}$.

4 Discussion

We have developed a mathematical model that describes the local distribution of a drug within a 3D brain unit as an extension of our earlier 2D proof-of-concept model [29]. The 3D brain unit is represented as a cube. This new model provides an important step towards more realistic features of the brain. The 3D representation allows for the representation of the brain ECF as continuous. The brain capillary blood flow and

active transport across the BBB have been explicitly incorporated. This enables us to more realistically predict the impact of the interplay of cerebral blood flow, BBB characteristics, brain ECF diffusion, brain ECF bulk flow and brain (target) binding on drug distribution within the brain. Altogether our model allows the study of the effect of a large amount of parameters values (summarized in Table 1) on drug distribution within the 3D brain unit.

This study has focused on the effect of the newly implemented brain properties on brain ECF concentrations a drug within the brain. It is shown that the brain capillary blood flow velocity and the passive BBB permeability affect the concentration of a drug within the brain, and, as anticipated [68, 69] that a low brain capillary blood flow velocity affects the short-term, but not the long-term concentration-time profiles of C_{pl} and C_{ECF}, (Fig 3 and 4). Also, passive BBB permeability has a high impact on brain ECF PK, even when drug is actively transported across the BBB. Moreover, the BBB permeability and, in smaller extent, the brain capillary blood flow velocity affect the impact of active influx on drug PK within the brain ECF (Fig 7 and 8). Interestingly, the brain capillary blood flow velocity, passive BBB permeability and active transport do not only affect the concentration of drug within the brain ECF, but also its distribution within the brain ECF (Fig 9 and 10.

Taken together, the 3D brain unit model shows the impact of drug-specific and brain-specific parameters on drug distribution within the brain ECF. The added value is that all these factors can now be studied *in conjunction* to understand the interdependencies of multiple brain parameter values and drug properties. This makes this single 3D brain unit model suitable for the next step, which is to mount up multiple units to represent a larger volume of brain tissue, in which the brain tissue properties for each unit can be defined independently. The units may be given different systemic properties (such as the BBB permeability or drug target concentration), to represent the heterogeneity of the brain in a 3D manner.

S1 Appendix - Nondimensionalization of the model

We can make Eq (2-16) dimensionless by introducing a change of variables. Here, the original variables are scaled to dimensionless variables by scaling with a characteristic, dimensional scale. We set:

$$
\begin{aligned}
t &= t_c\tau & D^* &= D_c d & k_{1\mathrm{on}} &= k_{1\mathrm{on_c}} K_{1\mathrm{on}} \\
x &= x_c\xi, & v &= v_c V & k_{1\mathrm{off}} &= k_{1\mathrm{off_c}} K_{1\mathrm{off}} \\
y &= y_c\eta & C_{\mathrm{pl}} &= C_{\mathrm{pl_c}} w & k_{2\mathrm{on}} &= k_{2\mathrm{on_c}} K_{2\mathrm{on}} \\
z &= z_c\zeta & C_{\mathrm{ECF}} &= C_{\mathrm{c}} u & k_{2\mathrm{off}} &= k_{2\mathrm{off_c}} K_{2\mathrm{off}} \\
B_1 &= B_{1_c} b_1 & B_1^{\max} &= B_{1_{\mathrm{c}}}^{\max} b_1^{\max} & P &= P_c p \\
B_2 &= B_{2_c} b_2 & B_2^{\max} &= B_{2_{\mathrm{c}}}^{\max} b_2^{\max} & SA_{\mathrm{BBB}} &= SA_{\mathrm{BBB_c}} sa_{\mathrm{BBB}} \\
T_{\mathrm{m}} &= T_{\mathrm{m_c}} t_{\mathrm{m}} & K_{\mathrm{m}} &= K_{\mathrm{m_c}} k_{\mathrm{m}} & v_{\mathrm{blood}} &= v_{\mathrm{blood_c}} V_{\mathrm{blood}}
\end{aligned}
$$

where

$$
\begin{aligned}
t_c &= 1s & D_c &= 10^{-10}\ \mathrm{m^2 s^{-1}} & k_{1\mathrm{on_c}} &= (\mu\mathrm{mol\ L^{-1}\ s})^{-1} \\
x_c &= 10^{-6}\ \mathrm{m} & v_c &= 10^{-6}\ \mathrm{m\ s^{-1}} & k_{1\mathrm{off_c}} &= 10^{-2}\ \mathrm{s^{-1}} \\
y_c &= 10^{-6}\ \mathrm{m} & C_{\mathrm{pl_c}} &= \mu\mathrm{mol\ L^{-1}} & k_{2\mathrm{on_c}} &= 10^{-2}\ (\mu\mathrm{mol\ L^{-1} s})^{-1} \\
z_c &= 10^{-6}\ \mathrm{m} & C_{\mathrm{c}} &= \mu\mathrm{mol\ L^{-1}} & k_{2\mathrm{off_c}} &= \mathrm{s^{-1}} \\
B_{1_c} &= \mu\mathrm{mol\ L^{-1}} & B_{2_c}^{\max} &= \mu\mathrm{mol\ L^{-1}} & P_c &= 10^{-7}\ \mathrm{m\ s^{-1}} \\
B_{2_c} &= \mu\mathrm{mol\ L^{-1}} & B_{2_c}^{\max} &= \mu\mathrm{mol\ L^{-1}} & SA_{\mathrm{BBB_c}} &= 10^{-6}\ \mathrm{L\ m^{-1}} \\
T_{\mathrm{m_c}} &= 10^{-7}\mu\mathrm{mol\ s^{-1}} & K_{\mathrm{m_c}} &= 10^{2}\ \mu\mathrm{mol\ L^{-1}} & v_{\mathrm{blood_c}} &= 10^{-3}\ \mathrm{m\ s^{-1}}
\end{aligned}
$$

This leads to the following dimensionless equation for drug in the blood plasma (example based on Eq (2), but similar for Eq (3)-(4)):

$$\frac{\partial w}{\partial \tau} = 10^3 V_{\mathrm{blood}} \frac{\partial w}{\partial \xi}$$

, and the following system of dimensionless equations for drug within the brain ECF (for Eq (6)):

$$
\begin{aligned}
\frac{\partial u}{\partial \tau} &= 10^2 d\left(\frac{\partial^2 u}{\partial \xi^2} + \frac{\partial^2 u}{\partial \eta^2} + \frac{\partial^2 u}{\partial \zeta^2}\right) - V\frac{\partial u}{\partial \xi} \\
&\quad - K_{1\mathrm{on}} u(b_1^{\max} - b_1) + 10^{-2} K_{1\mathrm{off}} b_1 \\
&\quad - 10^{-2} K_{2\mathrm{on}} u(b_2^{\max} - b_2) + K_{2\mathrm{off}} b_2 \\
\frac{\partial b_1}{\partial \tau} &= K_{1\mathrm{on}} u(b_1^{\max} - b_1) - 10^{-2} K_{1\mathrm{off}} b_1 \\
\frac{\partial b_2}{\partial \tau} &= 10^{-2} K_{2\mathrm{on}} u(b_2^{\max} - b_2) - K_{2\mathrm{off}} b_2.
\end{aligned}
$$

The corresponding boundary conditions (Eq (10)-(11), example for Eq (10), but similar for Eq (10)) are given by:

$$d\frac{\partial u}{\partial \xi} = 10^{-3} p(w - u(\xi,\eta,\zeta,\tau)) + \frac{10^{-1} t_{\mathrm{m}}}{s a_{\mathrm{BBB}}(k_{\mathrm{m}} + u(\xi,\eta,\zeta,\tau))} u(\xi,\eta,\zeta,\tau))$$

for ξ=0 and ξ=1.
The initial conditions become

$$w(\xi,\eta,\zeta,\tau=0) = 0$$

$$u(\xi,\eta,\zeta,\tau=0) = 0.$$

S2 Appendix- The effect of paracellular permeability on PK within the brain ECF

We study the passive transcellular permeability and passive paracellular permeability separately. This is different from before, where we have studied the total passive permeability. We study the effect of paracellular transport on the PK within the 3D brain unit. The paracellular permeability can increase due to disruption of the BBB, which in turn could be a result of disease. We include paracellular permeability and study its effect on drug concentrations within the 3D brain unit. For drugs for which the passive transcellular BBB permeability is low (P_{trans}=0.01·10^{-7} μmol s^{-1}),

Supplementary Figure 1. The PK in log-scale of unbound drug in the brain ECF (C_{ECF}) compared to the concentration of unbound drug in the blood plasma (C_{pl}, red curve). The transcellular passive permeability, P_{trans}, is set to $0.01{\cdot}10^{-7}$ m s^{-1} (left) and $1{\cdot}10^{-7}$ m s^{-1} (right), while the paracellular permeability, P_{para} is changed from 0 to $1{\cdot}10^{-1}$ m s^{-1} as depicted by different colours.

increasing has a large impact on drug PK within the brain (Fig 1, left). For drugs with a high passive permeability, an increased paracellular permeability has less effect, as shown in Fig 1(right). Essentially, changing the paracellular permeability has a similar effect as changing the total and the transcellular permeability: both increase the transport of drug along the concentration gradient between the blood plasma in the brain capillaries and the brain ECF.

S3 Appendix - The Renkin-Crone equation and the 3D brain unit model

We compare our model with the Renkin-Crone equation, which is a well-known equation relating blood flow to tissue uptake [64, 65], see Box I. The Renkin-Crone equation predicts that the transport of drugs across the BBB *into* the brain depends on the brain capillary blood flow rate, Q, in the presence of a large BBB permeability surface, PS. The volumetric parameters Q and PS are related to the brain capillary blood flow velocity, v_{blood}, and the BBB permeability, P, by the brain capillary and BBB surface area, SA_{cap} and SA_{BBB}, respectively. Here, we study the effect of v_{blood} on the passive transport of drug into the brain for different values of P. For this purpose, we:
1. Take a constant concentration of drug within the blood-plasma-domain (i.e. we set $C_{\mathrm{pl}}(\mathrm{t})=1$ for $C_{\mathrm{pl}}(\mathrm{t}) \in U_{\mathrm{in}}$.
2. We simplify boundary conditions (11) and (12) to $\frac{\partial C_{\mathrm{ECF}}}{\partial \mathrm{x}} = P(C_{\mathrm{pl}})$ in order to study passive *influx*, which is the passive movement of drug *into* the brain, only. Note that his is different from the approach we took previously, in which passive transport into or out of the brain ECF depends on a difference in concentration between the blood plasma and the brain ECF (see Eq(10)). Moreover, we set $T_{\text{m-in}}=0$ and $T_{\text{m-out}}=0$
3. We leave out drug binding and set ${B_1}^{\max}$, ${B_2}^{\max}=0$.
We measure the change in C_{ECF} ($\frac{\mathrm{d}C_{\mathrm{ECF}}}{\mathrm{dt}}$) at one specific point of the 3D brain unit, (x,y,z)=($\frac{3}{2}$r,$\frac{3}{2}$r, $\frac{3}{2}$r),which we denote by u_1, as indicated in Fig 2 (top). Similarly, we measure C_{pl} at one specific point of the 3D brain unit, (x,y,z)=($\frac{3}{2}$r,$\frac{1}{2}$r, $\frac{1}{2}$r), denoted by w_1, as indicated in Fig 2 (top). It takes some time until a steady state is reached and values of C_{pl} and $\frac{\mathrm{d}C_{\mathrm{ECF}}}{\mathrm{dt}}$ are approximately constant, see Fig 2 (bottom). At steady state k_{BBB}, which is the rate constant of drug transport from the blood plasma across the BBB into the brain ECF, can be determined as follows:

$$k_{\mathrm{bbb}} = \frac{\frac{\mathrm{d}C_{\mathrm{ECF}}}{\mathrm{dt}}(u_1)}{C_{\mathrm{pl}}(w_1)} \tag{1}$$

, with $\frac{\mathrm{d}C_{\mathrm{ECF}}}{\mathrm{dt}}(u_1)$ the change in C_{ECF} over time in u_1 and $C_{\mathrm{pl}}(w_1)$ the value of C_{pl} in w_1 when both $C_{\mathrm{pl}}(w_1)$ and $\frac{\mathrm{d}C_{\mathrm{ECF}}}{\mathrm{dt}}$ (u_1) do not longer vary. Fig 3 demonstrates that the way v_{blood} affects k_{BBB} varies with the value of P. With values of P of $1{\cdot}10^{-4}$ m s^{-1} or lower, k_{BBB} is independent of v_{blood}. With values of P of $10{\cdot}10^{-4}$ m s^{-1} or higher, k_{BBB} linearly increases with v_{blood} up to a certain threshold (e.g. for $P=10{\cdot}10^{-4}$ m s^{-1}, k_{BBB} starts to approach constant levels when $v_{\mathrm{blood}}\geq 2$). These results correspond to the predictions of the Renkin-Crone equation (Box I).

Supplementary Figure 2. Determination of $C_{\mathrm{pl}}(w_1)$ and $\frac{\mathrm{dC_{ECF}}}{\mathrm{dt}}(u_1)$. Time Top: Locations of w_1 and u_1, where $C_{\mathrm{pl}}(w_1)$and $\frac{\mathrm{dC_{ECF}}}{\mathrm{dt}}(u_1)$ are measured, within the 3D brain unit. The black arrow indicates the direction of the brain capillary blood flow, while the green arrow indicates the direction of BBB transport. Bottom: Profiles of C_{pl} (w_1) and $\frac{\mathrm{dC_{ECF}}}{\mathrm{dt}}(u_1)$ over time.

Supplementary Figure 3. The effects of v_{blood} on k_{BBB}. The effect of v_{blood} on k_{BBB} depends on P. Note that here P is taken 10^3 times its default value, see Table 2.

Box I - The Renkin-Crone equation

The brain capillary blood flow affects the passive clearance of a drug across the BBB according to the Renkin-Crone equation [64,65]. The Renkin-Crone equation describes the relation between the brain capillary blood flow and transport across the BBB as follows:

$$K_{\mathrm{in}} = QE \quad \text{with } E = 1 - e^{\frac{-PS}{Q}} \tag{2}$$

, with K_{in} the passive clearance of drug from the blood into the brain (L s^{-1}), Q (L s^{-1}) the blood flow rate in the brain capillaries and PS (L s^{-1}) the passive permeability surface of the BBB. Both Q and PS have the same units, such that, E, the ratio of compound extracted from the blood into the brain, is dimensionless. The Renkin-Crone equation shows that the transport from the blood into the brain depends on the ratio of the BBB permeability surface (PS) and the blood flow rate (Q). When $PS \gg Q$, the extraction ratio E approaches 1, such that K_{in} is determined by changes in Q. In other words, when $PS \gg Q$, drug transport across the BBB is much faster than the rate of drug supply into the brain capillaries. Then, drug transport into the brain can only be increased by increasing Q. On the other hand, when $Q \gg PS$, E approaches 0. In this case, the drug supply into the brain capillaries is much faster than the rate of drug transport across the BBB. Then, drug transport into the brain can only be increased by increasing PS.
The Renkin-Crone equation implies that the effect of the brain capillary blood flow rate on the concentration of unbound drug exchanging with the brain is most pronounced for drugs that easily cross the BBB [65, 70], i.e. drugs for which $PS \gg Q$, or, in terms of velocity rather than rate, drugs for which $P \gg v_{\mathrm{blood}}$. Under general, non-pathological circumstances v_{blood} is around $5{\cdot}10^{-4}$ m s^{-1} (see Tables 1 and 2), which implies that BBB transport is impacted by the blood flow velocity when drug molecules have a value of P that is (much) higher than 10^{-4} m s^{-1} (i.e. 10^3 times the default value as given in Table 2).

506

References

1. Vendel E, Rottschäfer V, de Lange ECM. The need for mathematical modelling of spatial drug distribution within the brain Fluid and Barriers of the CNS. 2019;16:12.

2. Summerfield SG, Stevens AJ, Cutler L, del Carmen Osuna M, Hammond B, Tang SP, et al. Improving the in vitro prediction of in vivo central nervous system penetration: integrating permeability, P-glycoprotein efflux, and free fractions in blood and brain. Journal of Pharmacology and Experimental Therapeutics. 2006;316(3):1282–1290.

3. Summerfield S, Lucas A, Porter R, Jeffrey P, Gunn R, Read K, et al. Toward an improved prediction of human in vivo brain penetration. Xenobiotica. 2008;38(12):1518–1535.

4. Tsuji A. Small molecular drug transfer across the blood-brain barrier via carrier-mediated transport systems. NeuroRx. 2005;2(1):54–62.

5. Van Bree J, De Boer A, Danhof M, Ginsel L, Breimer D. Characterization of an" in vitro" blood-brain barrier: effects of molecular size and lipophilicity on cerebrovascular endothelial transport rates of drugs. Journal of Pharmacology and Experimental Therapeutics. 1988;247(3):1233–1239.

6. Hammarlund-Udenaes M, Paalzow LK, de Lange EC. Drug Equilibration Across the Bloodâ€"Brain Barrier-Pharmacokinetic Considerations Based on the Microdialysis Method. Pharmaceutical research. 1997;14(2):128–134.

7. Waterhouse RN. Determination of lipophilicity and its use as a predictor of blood–brain barrier penetration of molecular imaging agents. Molecular Imaging & Biology. 2003;5(6):376–389.

8. Löscher W, Potschka H. Role of drug efflux transporters in the brain for drug disposition and treatment of brain diseases. Progress in neurobiology. 2005;76(1):22–76.

9. Syvänen S, Xie R, Sahin S, Hammarlund-Udenaes M. Pharmacokinetic consequences of active drug efflux at the blood–brain barrier. Pharmaceutical research. 2006;23(4):705–717.

10. Watanabe T, Kusuhara H, Maeda K, Shitara Y, Sugiyama Y. Physiologically based pharmacokinetic modeling to predict transporter-mediated clearance and distribution of pravastatin in humans. Journal of Pharmacology and Experimental Therapeutics. 2009;328(2):652–662.

11. Nicholson C, Phillips J. Ion diffusion modified by tortuosity and volume fraction in the extracellular microenvironment of the rat cerebellum. The Journal of Physiology. 1981;321:225.

12. Nicholson C. Diffusion and related transport mechanisms in brain tissue. Reports on progress in Physics. 2001;64(7):815.

13. Wang Y, Welty DR. The simultaneous estimation of the influx and efflux blood-brain barrier permeabilities of gabapentin using a microdialysis-pharmacokinetic approach. Pharmaceutical research. 1996;13(3):398–403.

14. Liu X, Vilenski O, Kwan J, Apparsundaram S, Weikert R. Unbound brain concentration determines receptor occupancy: a correlation of drug concentration and brain serotonin and dopamine reuptake transporter occupancy for eighteen compounds in rats. Drug metabolism and disposition. 2009;37(7):1548–1556. doi:10.1016/j.jconrel.2015.09.025.

15. Vauquelin G. On the â€˜microâ€™-pharmacodynamic and pharmacokinetic mechanisms that contribute to long-lasting drug action. Expert Opinion on Drug Discovery. 2015;10(10):1085–1098.

16. de Witte WEA, Danhof M, van der Graaf PH, de Lange ECM. In vivo Target Residence Time and Kinetic Selectivity: The Association Rate Constant as Determinant. Trends in Pharmacological Sciences. 2016;37(10):831–842. doi:10.1016/j.tips.2016.06.008.

17. Pan AC, Borhani DW, Dror RO, Shaw DE. Molecular determinants of drugâ€“receptor binding kinetics. Drug discovery today. 2013;18(13-14):667–673.

18. Collins JM, Dedrick RL. Distributed model for drug delivery to CSF and brain tissue. American Journal of Physiology-Regulatory, Integrative and Comparative Physiology. 1983;245(3):R303–R310.

19. de Lange EC, Ravenstijn PG, Groenendaal D, van Steeg TJ. Toward the prediction of CNS drug-effect profiles in physiological and pathological conditions using microdialysis and mechanism-based pharmacokinetic-pharmacodynamic modeling. The AAPS journal. 2005;7(3):E532–E543.

20. Ball K, Bouzom F, Scherrmann JM, Walther B, DeclÃ¨ves X. A Physiologically Based Modeling Strategy during Preclinical CNS Drug Development. Molecular Pharmaceutics. 2014;11(3):836–848. doi:10.1021/mp400533q.

21. Nhan T, Burgess A, Lilge L, Hynynen K. Modeling localized delivery of Doxorubicin to the brain following focused ultrasound enhanced blood-brain barrier permeability. Physics in Medicine and Biology. 2014;59(20):5987.

22. Calvetti D, Cheng Y, Somersalo E. A spatially distributed computational model of brain cellular metabolism. Journal of theoretical biology. 2015;376:48–65.

23. Ehlers W, Wagner A. Multi-component modelling of human brain tissue: a contribution to the constitutive and computational description of deformation, flow and diffusion processes with application to the invasive drug-delivery problem. Computer methods in biomechanics and biomedical engineering. 2015;18(8):861–879.

24. Trapa PE, Belova E, Lira JL, Scott DO, Steyn SJ. Insights from an integrated physiologically based pharmacokinetic model for brain penetration. Journal of pharmaceutical sciences. 2016;105(2):965–971.

25. Gaohua L, Neuhoff S, Johnson TN, Rostami-Hodjegan A, Jamei M. Development of a permeability-limited model of the human brain and cerebrospinal fluid (CSF) to integrate known physiological and biological knowledge: estimating time varying CSF drug concentrations and their variability using in vitro data. Drug metabolism and pharmacokinetics. 2016;31(3):224–233.

26. Zhan W, Arifin DY, Lee TKY, Wang CH. Mathematical modelling of convection enhanced delivery of Carmustine and paclitaxel for brain tumour therapy. Pharmaceutical Research. 2017;34(4):860–873.

27. Yamamoto Y, Välitalo PA, Huntjens DR, Proost JH, Vermeulen A, Krauwinkel W, et al. Predicting Drug Concentration-Time Profiles in Multiple CNS Compartments Using a Comprehensive Physiologically-Based Pharmacokinetic Model. CPT: pharmacometrics & systems pharmacology. 2017;6(11):765–777.

28. Yamamoto Y, Välitalo PA, Wong YC, Huntjes DR, Proost JH, Vermeulen A, et al. Prediction of human CNS pharmacokinetics using a physiologically-based pharmacokinetic modeling approach. European Journal of Pharmaceutical Sciences. 2018;112:168–179.

29. Vendel E, Rottschäfer V, de Lange ECM. Improving the Prediction of Local Brain Distribution Profiles with a New Mathematical Model. Bulletin for Mathematical Biology, Special Issue on "Mathematics to Support Drug Discovery and Development". 2018; p. 1–31.

30. Rowland M, Tozer TN. Clinical pharmacokinetics/pharmacodynamics. Lippincott Williams and Wilkins Philadelphia; 2005.

31. Jucker M, Bättig K, Meier-Ruge W. Effects of aging and vincamine derivatives on pericapillary microenvironment: stereological characterization of the cerebral capillary network. Neurobiology of aging. 1990;11(1):39–46.

32. Schlageter KE, Molnar P, Lapin GD, Groothuis DR. Microvessel organization and structure in experimental brain tumors: microvessel populations with distinctive structural and functional properties. Microvascular research. 1999;58(3):312–328.

33. Pardridge WM. The blood-brain barrier: bottleneck in brain drug development. NeuroRx. 2005;2(1):3–14.

34. Tata D, Anderson B. A new method for the investigation of capillary structure. Journal of neuroscience methods. 2002;113(2):199–206.

35. McGinty S, Pontrelli G. On the role of specific drug binding in modelling arterial eluting stents. Journal of Mathematical Chemistry. 2016;54(4):967–976. doi:10.1007/s10910-016-0618-7.

36. Tzafriri AR, Groothuis A, Price GS, Edelman ER. Stent elution rate determines drug deposition and receptor-mediated effects. Journal of Controlled Release. 2012;161(3):918–926.

37. Schiesser WE, Griffiths GW. A compendium of partial differential equation models: method of lines analysis with Matlab. Cambridge University Press; 2009.

38. Tasso L, Bettoni CC, Costa TD. Pharmacokinetic plasma profile and bioavailability evaluation of gatifloxacin in rats. Latin American Journal of Pharmacy. 2008;27(2):270–273.

39. Karbowski J. Scaling of brain metabolism and blood flow in relation to capillary and neural scaling. PloS one. 2011;6(10):e26709.

40. Nicholson C, Chen KC, Hrabětová S, Tao L. Diffusion of molecules in brain extracellular space: theory and experiment. Progress in brain research. 2000;125:129–154.

41. Nicholson C, Kamali-Zare P, Tao L. Brain Extracellular Space as a Diffusion Barrier. Comput Vis Sci. 2011;14(7):309–325. doi:10.1038/nature13314.A.

42. Saltzman W. Interstitial transport in the brain: principles for local drug delivery. The biomedical engineering handbook, 2nd edn CRC, Boca Raton. 2000;.

43. Hladky SB, Barrand MA. Mechanisms of fluid movement into, through and out of the brain: evaluation of the evidence. Fluids and Barriers of the CNS. 2014;11(1):1.

44. Wong A, Ye M, Levy A, Rothstein J, Bergles D, Searson PC. The blood-brain barrier: an engineering perspective. Frontiers in neuroengineering. 2013;6:7.

45. Lentz KA, Polli JW, Wring SA, Humphreys JE, Polli JE. Influence of passive permeability on apparent P-glycoprotein kinetics. Pharmaceutical research. 2000;17(12):1456–1460.

46. Hoffmann J, Fichtner I, Lemm M, Lienau P, Hess-Stumpp H, Rotgeri A, et al. Sagopilone crosses the blood–brain barrier in vivo to inhibit brain tumor growth and metastases. Neuro-oncology. 2009;11(2):158–166.

47. Takasato Y, Rapoport SI, Smith QR. An in situ brain perfusion technique to study cerebrovascular transport in the rat. American Journal of Physiology-Heart and Circulatory Physiology. 1984;247(3):H484–H493.

48. Liu X, Tu M, Kelly RS, Chen C, Smith BJ. Development of a computational approach to predict blood-brain barrier permeability. Drug metabolism and disposition. 2004;32(1):132–139.

49. Youdim KA, Qaiser MZ, Begley DJ, Rice-Evans CA, Abbott NJ. Flavonoid permeability across an in situ model of the blood–brain barrier. Free Radical Biology and Medicine. 2004;36(5):592–604.

50. Summerfield SG, Read K, Begley DJ, Obradovic T, Hidalgo IJ, Coggon S, et al. Central nervous system drug disposition: the relationship between in situ brain permeability and brain free fraction. Journal of Pharmacology and Experimental Therapeutics. 2007;322(1):205–213.

51. Bruns RF, Daly JW, Snyder SH. Adenosine receptors in brain membranes: binding of N6-cyclohexyl [3H] adenosine and 1, 3-diethyl-8-[3H] phenylxanthine. Proceedings of the National Academy of Sciences. 1980;77(9):5547–5551.

52. Perry DC, Mullis KB, Øie S, Sadée W. Opiate antagonist receptor binding in vivo: evidence for a new receptor binding model. Brain research. 1980;199(1):49–61.

53. Farde L, Eriksson L, Blomquist G, Halldin C. Kinetic analysis of central [11C] raclopride binding to D2-dopamine receptors studied by PETâ€"a comparison to the equilibrium analysis. Journal of Cerebral Blood Flow & Metabolism. 1989;9(5):696–708.

54. Levy G. Pharmacologic target-mediated drug disposition. Clinical Pharmacology & Therapeutics. 1994;56(3):248–252.

55. Costes N, Merlet I, Zimmer L, Lavenne F, Cinotti L, Delforge J, et al. Modeling [18F] MPPF positron emission tomography kinetics for the determination of 5-hydroxytryptamine (1A) receptor concentration with multiinjection. Journal of Cerebral Blood Flow & Metabolism. 2002;22(6):753–765.

56. Millet P, Graf C, Moulin M, Ibáñez V. SPECT quantification of benzodiazepine receptor concentration using a dual-ligand approach. Journal of Nuclear Medicine. 2006;47(5):783–792.

57. Dahl G, Akerud T. Pharmacokinetics and the drug–target residence time concept. Drug Discovery Today. 2013;18(15-16):697–707.

58. Ivanov K, Kalinina M, Levkovich YI. Blood flow velocity in capillaries of brain and muscles and its physiological significance. Microvascular research. 1981;22(2):143–155.

59. Hudetz AG, Biswal BB, Fehér G, Kampine JP. Effects of hypoxia and hypercapnia on capillary flow velocity in the rat cerebral cortex. Microvascular research. 1997;54(1):35–42.

60. Seylaz J, Charbonné R, Nanri K, Von Euw D, Borredon J, Kacem K, et al. Dynamic in vivo measurement of erythrocyte velocity and flow in capillaries and of microvessel diameter in the rat brain by confocal laser microscopy. Journal of Cerebral Blood Flow & Metabolism. 1999;19(8):863–870.

61. Hutchinson EB, Stefanovic B, Koretsky AP, Silva AC. Spatial flow-volume dissociation of the cerebral microcirculatory response to mild hypercapnia. Neuroimage. 2006;32(2):520–530.

62. Itoh Y, Suzuki N. Control of brain capillary blood flow. Journal of Cerebral Blood Flow & Metabolism. 2012;32(7):1167–1176.

63. Villringer A, Them A, Lindauer U, Einhäupl K, Dirnagl U. Capillary perfusion of the rat brain cortex. An in vivo confocal microscopy study. Circulation research. 1994;75(1):55–62.

64. Renkin EM. Transport of potassium-42 from blood to tissue in isolated mammalian skeletal muscles. American Journal of Physiology-Legacy Content. 1959;197(6):1205–1210.

65. Crone C. The permeability of capillaries in various organs as determined by use of the â€˜indicator diffusionâ€™method. Acta Physiologica. 1963;58(4):292–305.

66. Mikitsh JL, Chacko AM. Pathways for small molecule delivery to the central nervous system across the blood-brain barrier. Perspectives in medicinal chemistry. 2014;6:11.

67. Stamatovic SM, Keep RF, Andjelkovic AV. Brain endothelial cell-cell junctions: how to "open" the blood brain barrier. Current neuropharmacology. 2008;6(3):179–192.

68. Banks WA. Characteristics of compounds that cross the blood-brain barrier. BMC neurology. 2009;9(1):S3.

69. Hammarlund-Udenaes M, Fridén M, Syvänen S, Gupta A. On the rate and extent of drug delivery to the brain. Pharmaceutical research. 2008;25(8):1737–1750.

70. Pardridge WM. CSF, blood-brain barrier, and brain drug delivery. Expert opinion on drug delivery. 2016;13(7):963–975.

71. Conant GC, Wolfe KH. Turning a hobby into a job: how duplicated genes find new functions. Nat Rev Genet. 2008 Dec;9(12):938–950.

72. Ohno S. Evolution by gene duplication. London: George Alien & Unwin Ltd. Berlin, Heidelberg and New York: Springer-Verlag.; 1970.

73. Magwire MM, Bayer F, Webster CL, Cao C, Jiggins FM. Successive increases in the resistance of Drosophila to viral infection through a transposon insertion followed by a Duplication. PLoS Genet. 2011 Oct;7(10):e1002337.

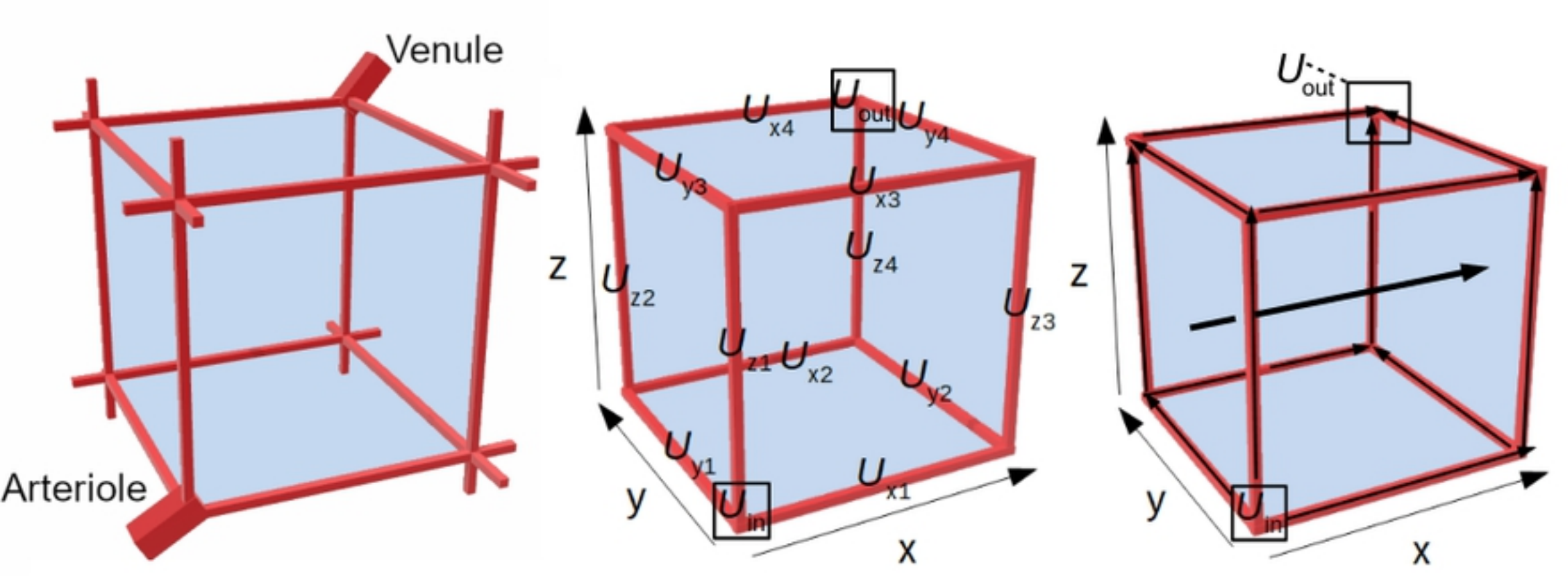
Venule
Arteriole
z
y
x
U_{out}
U_{x4}
U_{y4}
U_{y3}
U_{x3}
U_{z4}
U_{z2}
U_{z3}
U_{z1}
U_{x2}
U_{y2}
U_{y1}
U_{x1}
U_{in}

Figure 1

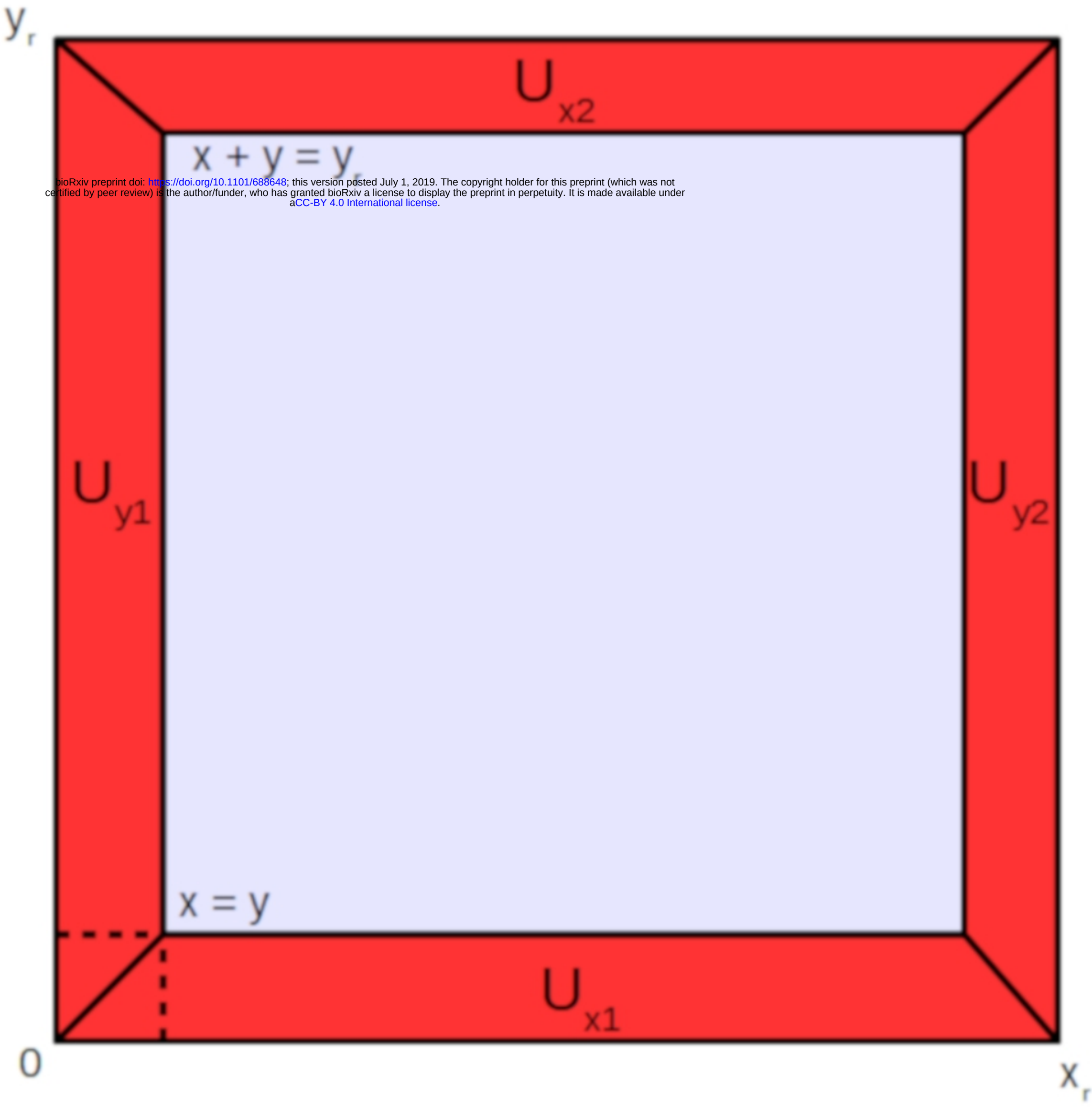

Figure 2

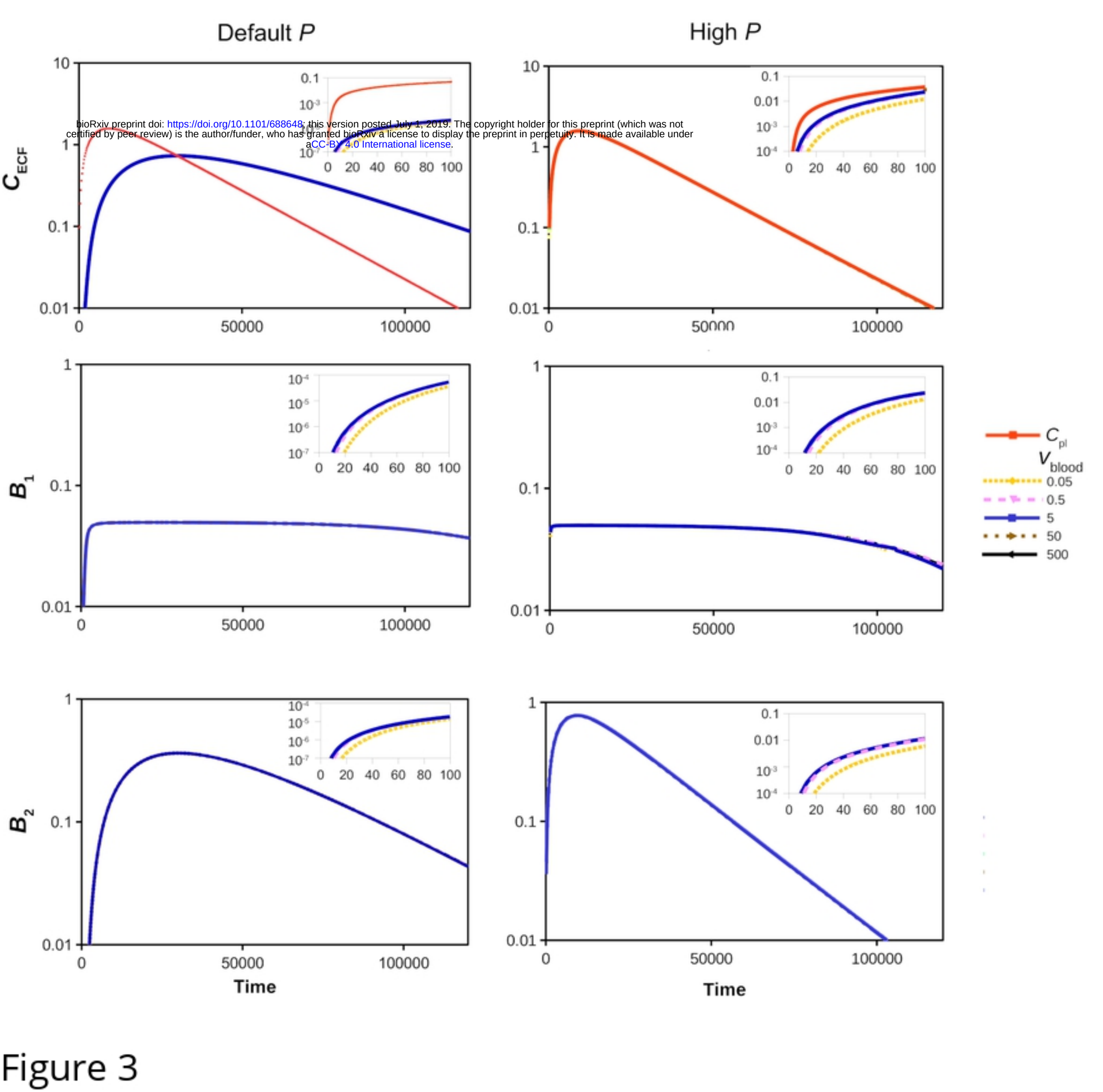

Figure 3

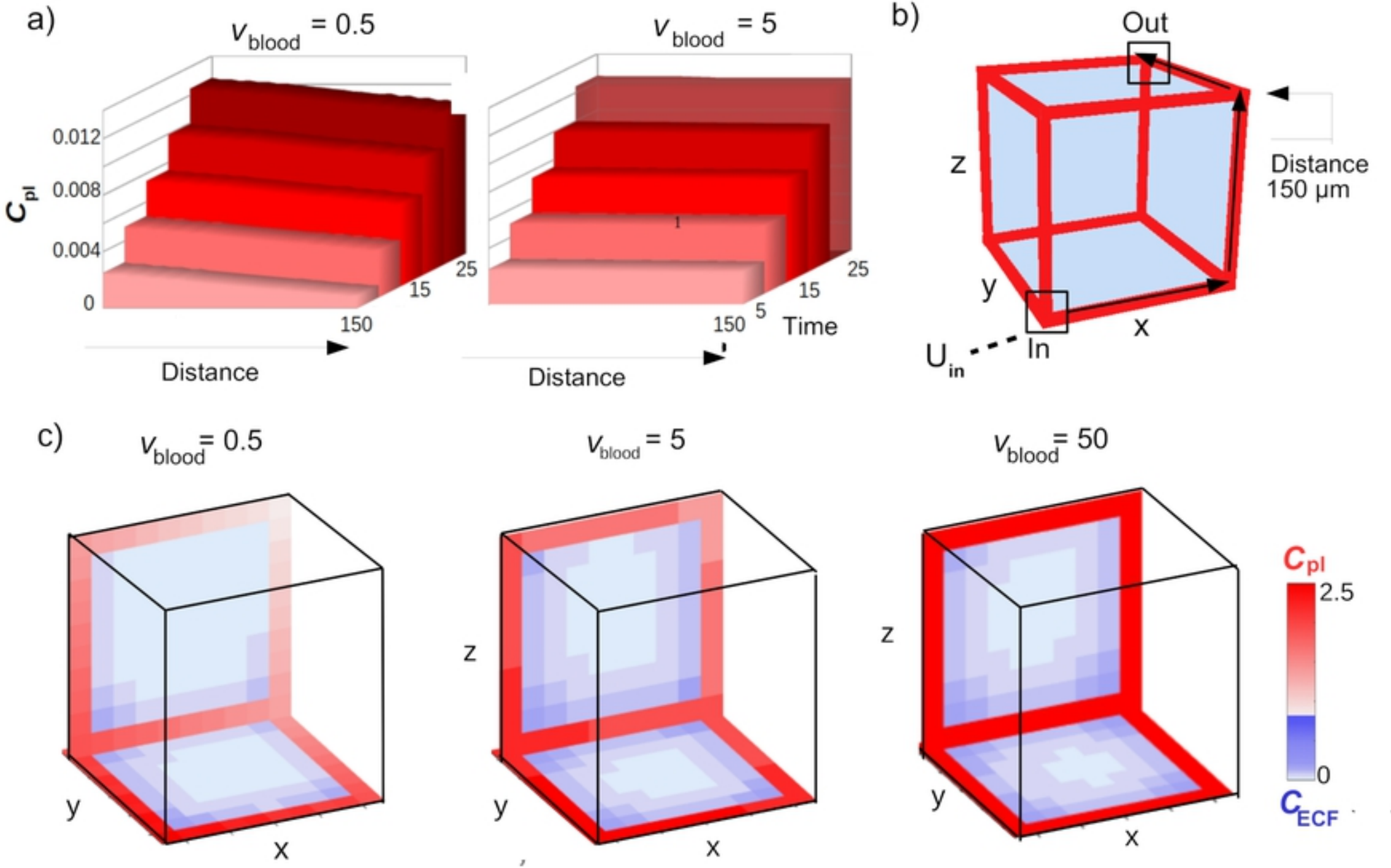
a)
v_{blood} = 0.5
v_{blood} = 5
C_{pl}
0.012
0.008
0.004
0
150
15
25
5
Time
Distance
b)
Out
In
U_{in}
z
y
x
Distance
150 µm
c)
v_{blood} = 0.5
v_{blood} = 5
v_{blood} = 50
C_{pl}
2.5
0
C_{ECF}

Figure 4

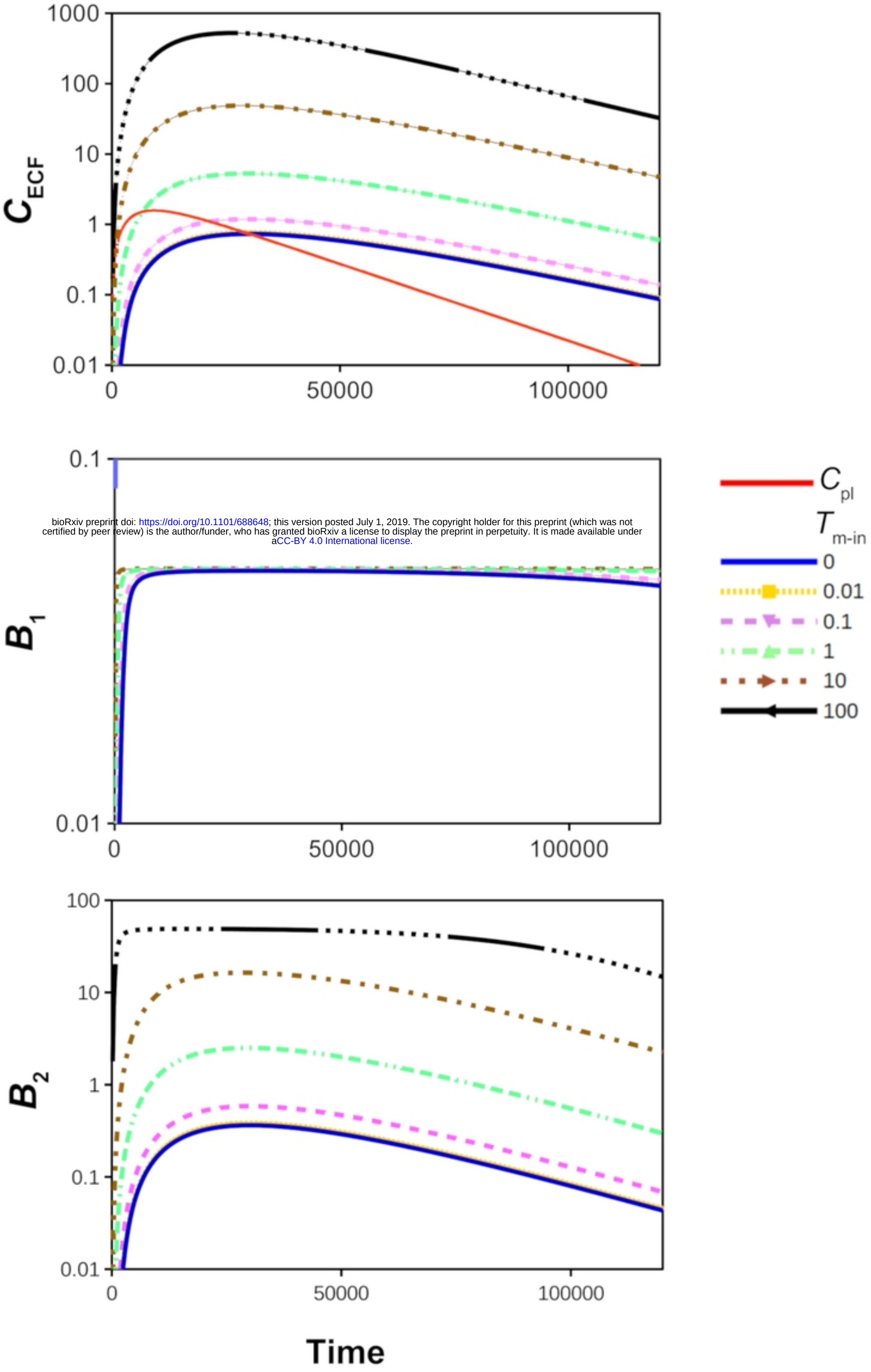

Figure 5

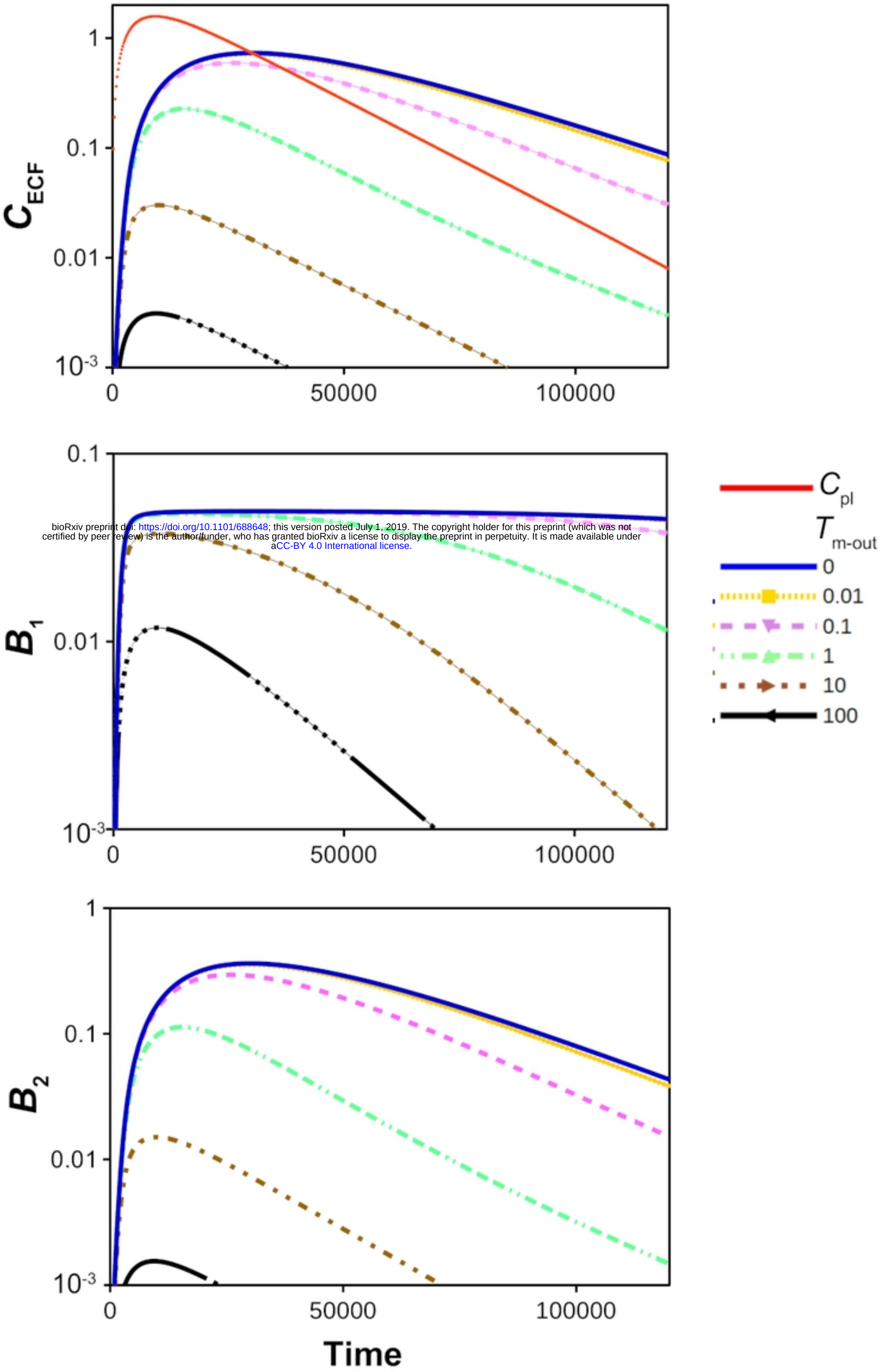

Figure 6

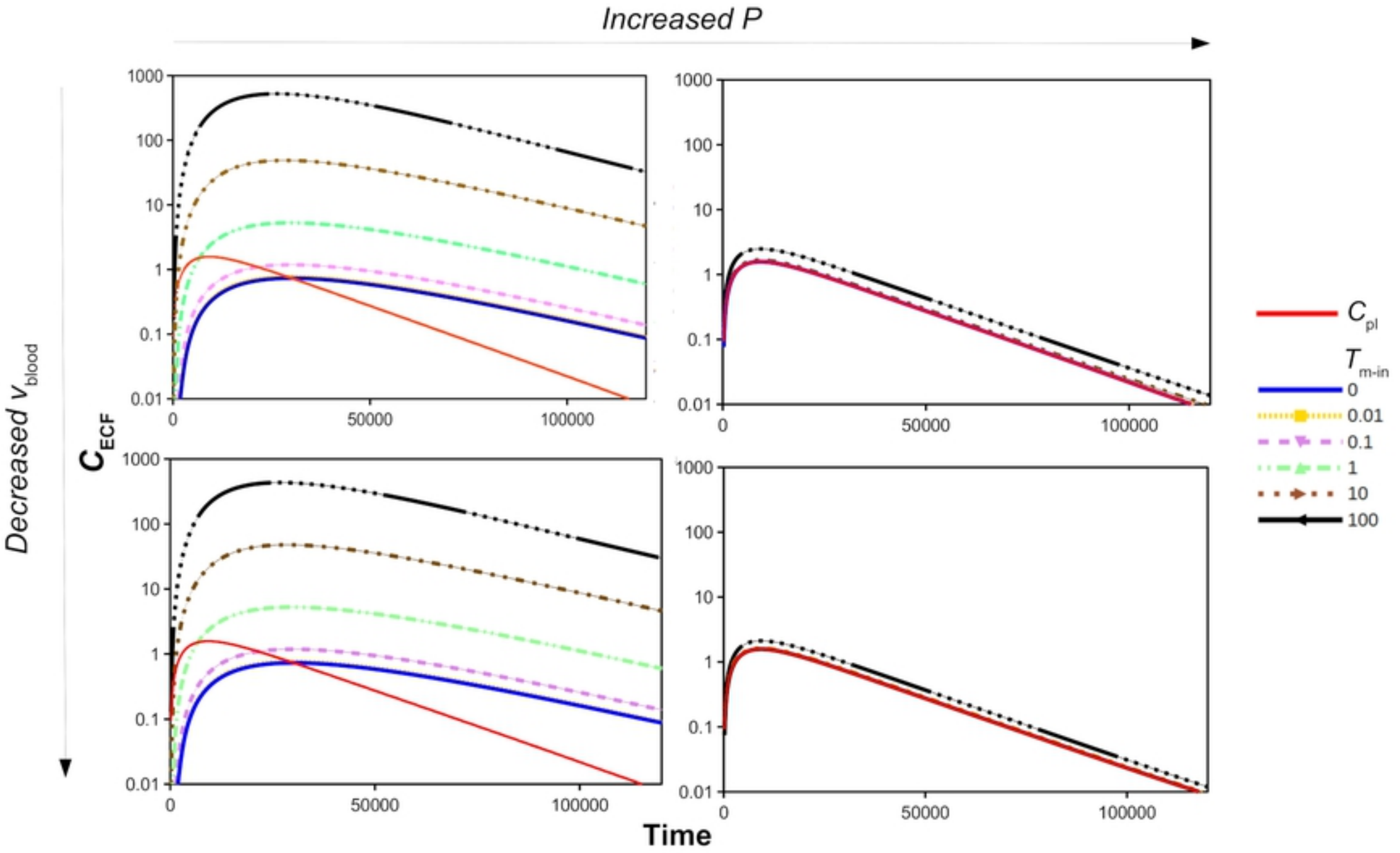
Increased P
Decreased v_{blood}
C_{ECF}
Time
1000
100
10
1
0.1
0.01
0
50000
100000
C_{pl}
$T_{m\text{-}in}$
0
0.01
0.1
1
10
100

Figure 7

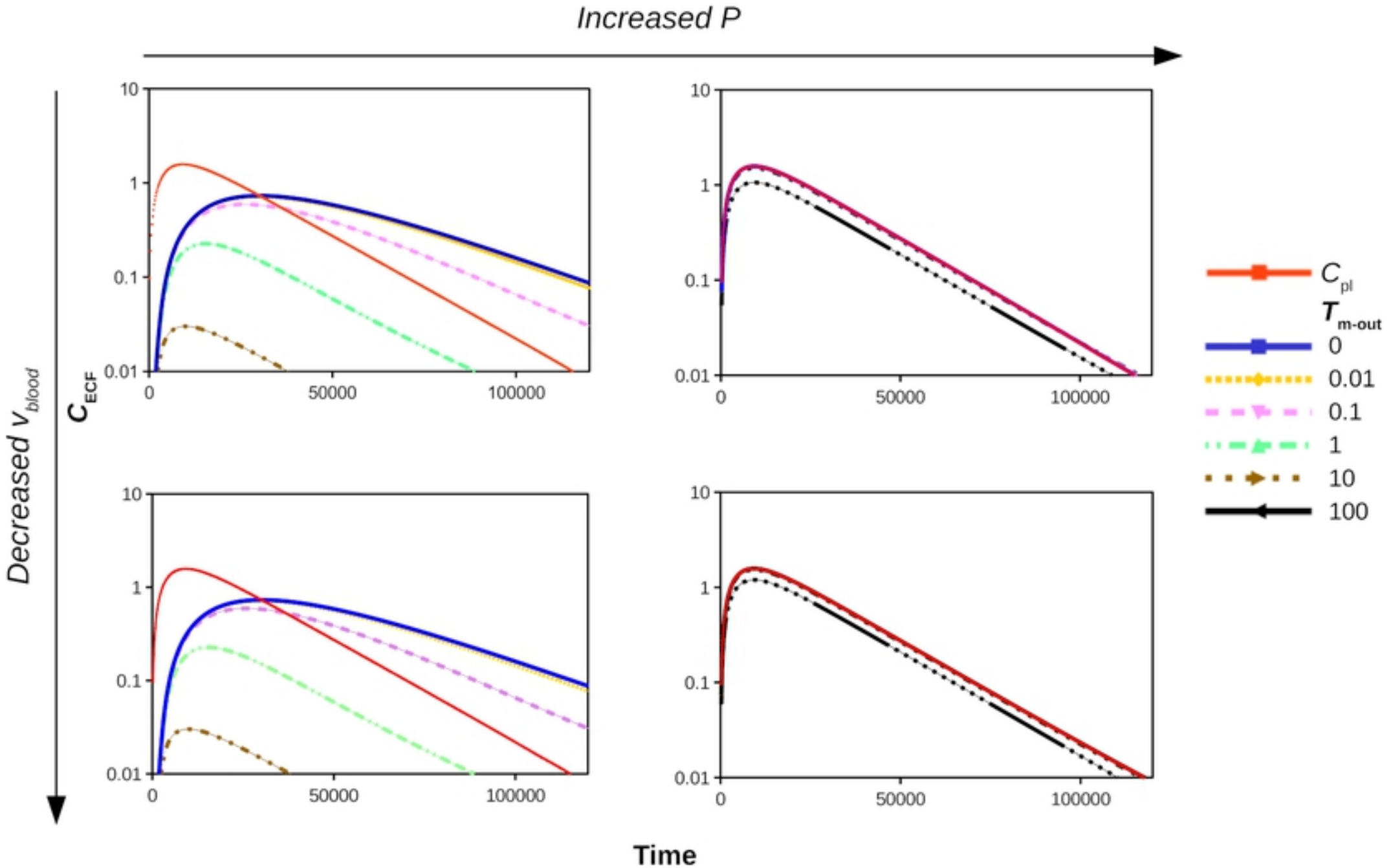
Increased P
Decreased v_{blood}
C_{ECF}
Time
10
1
0.1
0.01
0
50000
100000
C_{pl}
$T_{m\text{-}out}$
0
0.01
0.1
1
10
100

Figure 8

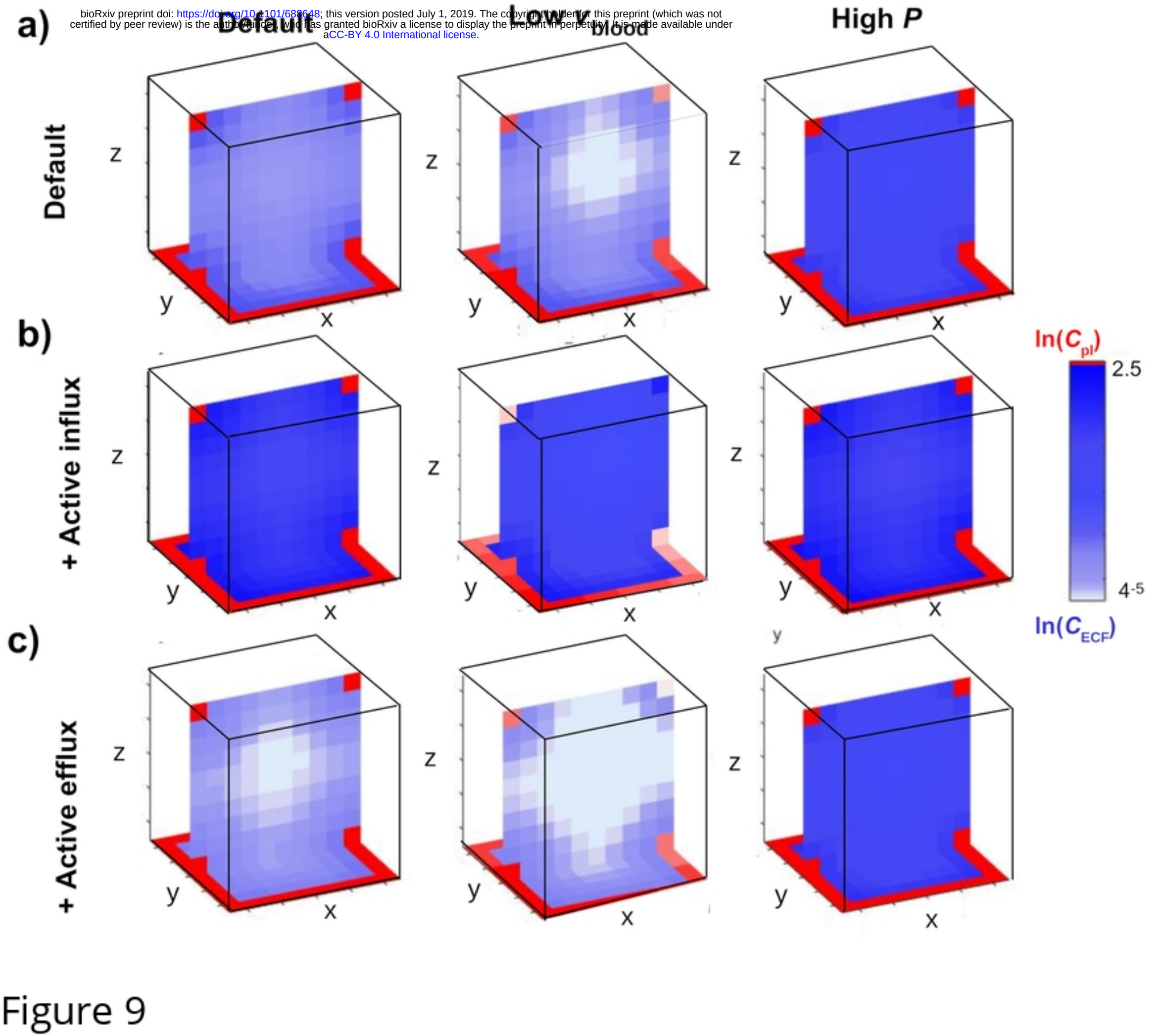

Figure 9

a)

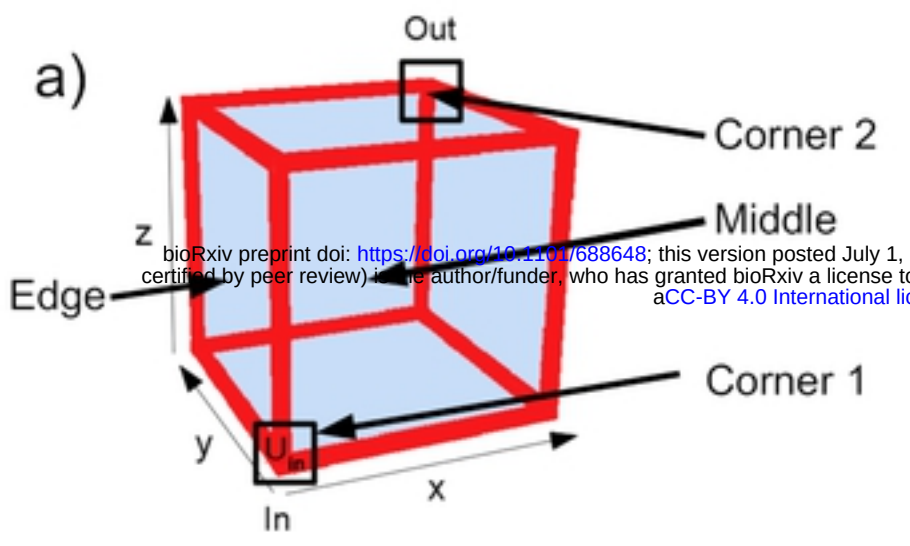

c)

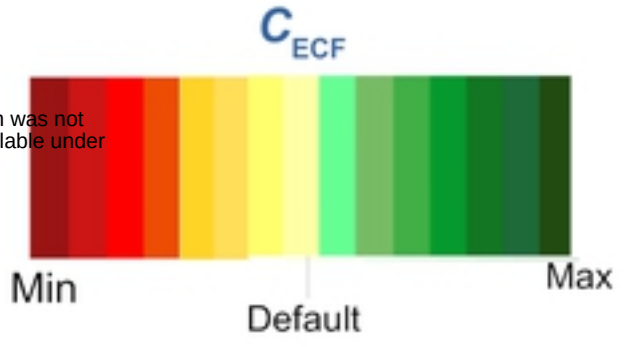

b)

P = 0.1

T_m	v_{blood} = 0.5				v_{blood} = 5				v_{blood} = 50			
	Corner 1	Edge	Middle	Corner 2	Corner 1	Edge	Middle	Corner 2	Corner 1	Edge	Middle	Corner 2
100	1030	983.3	972.6	1010	1269	1221	1209	1246	1297	1249	1237	1273
10	101.1	96.29	95.07	98.76	104.4	99.58	98.35	102.1	104.8	99.92	98.68	102.4
1	5.864	5.32	5.184	5.633	5.908	5.364	5.228	5.681	5.913	5.369	5.233	5.685
0	0.6834	0.6204	0.6069	0.6932	0.6864	0.6233	0.601	0.6968	0.6867	0.6236	0.6102	0.6972
1	0.6749	0.613	0.5997	0.6851	0.6778	0.616	0.6027	0.6886	0.6781	0.6163	0.603	0.689
10	0.6061	0.5537	0.5416	0.6191	0.6084	0.556	0.5441	0.6221	0.6087	0.5563	0.5443	0.6224
100	0.2871	0.2733	0.2665	0.308	0.2877	0.2741	0.2673	0.3092	0.2878	0.2842	0.2674	0.3094

Inward: 100, 10, 1, 0 — Outward: 1, 10, 100

P = 1

	Corner 1	Edge	Middle	Corner 2	Corner 1	Edge	Middle	Corner 2	Corner 1	Edge	Middle	Corner 2
100	993.8	949.5	939.1	974.2	1222	1177	1165	1198	1249	1204	1192	1225
10	114	108.9	107.6	111.7	117.7	112.6	111.3	115.4	118.1	113	111.7	115.8
1	15.75	14.66	14.41	15.6	15.9	14.81	14.56	15.76	15.91	14.83	14.58	15.77
0	8.422	7.802	7.672	8.519	8.476	7.857	7.727	8.581	8.481	7.862	7.733	8.587
1	8.284	7.679	7.55	8.386	8.336	7.731	7.603	8.445	8.341	7.736	7.609	8.451
10	7.207	6.713	6.6	7.345	7.242	6.748	6.636	7.387	7.245	6.752	6.64	7.391
100	3.015	2.908	2.845	3.233	3.017	2.91	2.848	3.241	3.018	2.911	2.849	3.242

Inward: 100, 10, 1 — Outward: 0, 1, 10, 100

P = 10

T_m	Corner 1	Edge	Middle	Corner 2	Corner 1	Edge	Middle	Corner 2	Corner 1	Edge	Middle	Corner 2
100	740	707.1	699.2	719.1	892.2	862.2	853.9	867.2	909.7	880.1	871.7	884.3
10	189.6	183.6	182.1	187.5	194.9	189	187.6	192.9	195.5	189.6	188.1	193.4
1	121.9	118.3	117.5	122.1	123.2	119.7	118.9	123.5	123.4	120	119.1	123.6
0	114.2	110.9	110.2	114.6	115.2	112	111.2	115.7	115.3	112.1	111.4	115.8
1	111.9	108.8	108.1	112.4	112.8	109.7	109	113.4	112.9	109.8	109.1	113.5
10	94.49	92.32	91.74	95.55	94.68	92.53	91.96	95.81	94.7	92.55	91.98	95.84
100	33.91	34.28	33.94	36.06	33.31	33.57	33.24	35.52	33.25	33.5	33.17	35.47

Inward: 100, 10, 1, 0 — Outward: 1, 10, 100

Figure 10

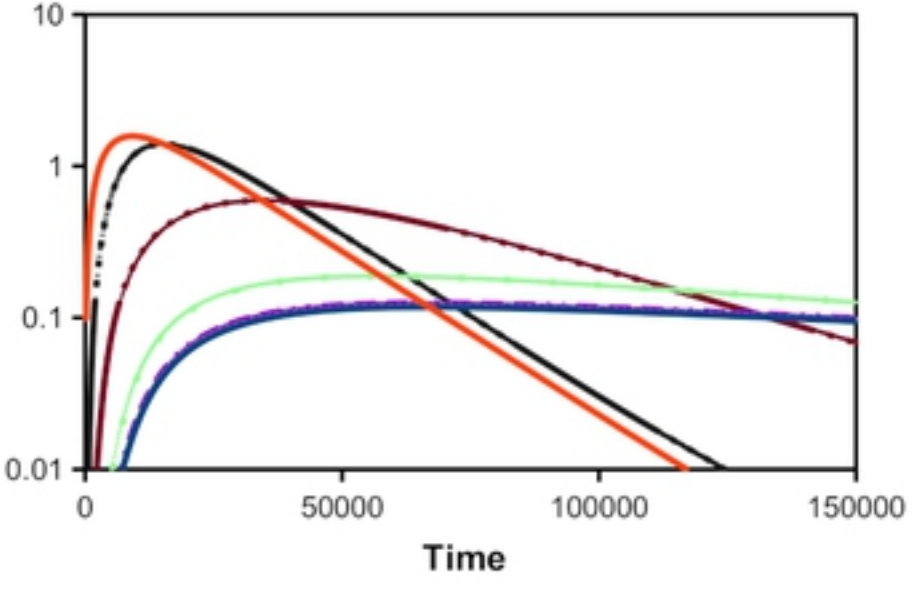

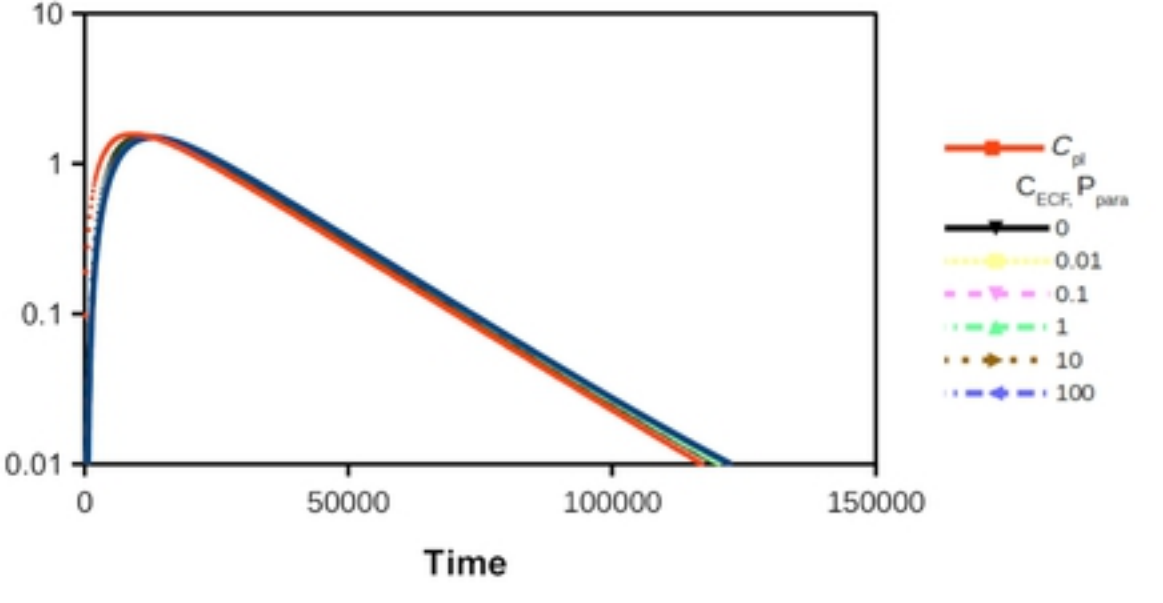

Supplementary Figure 1

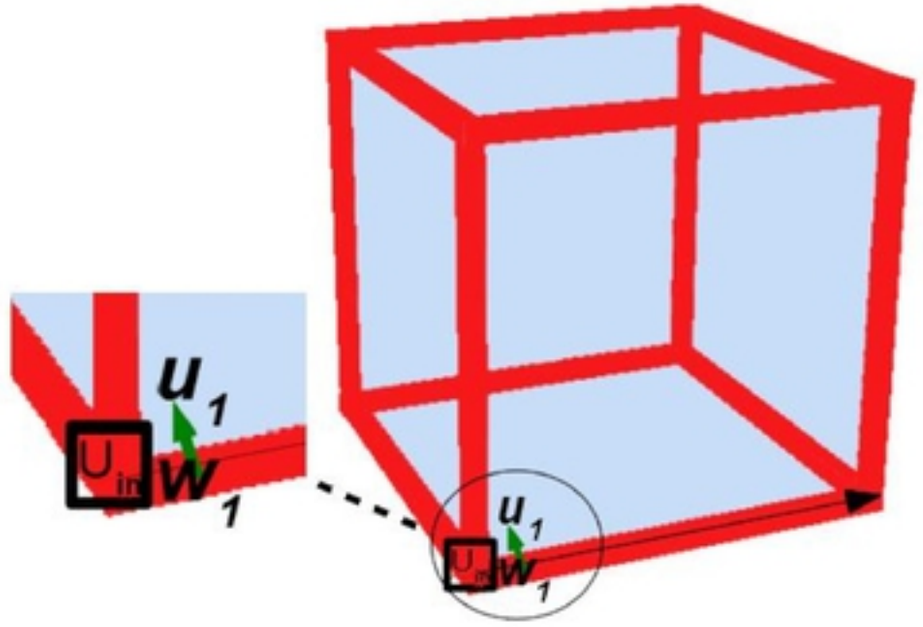

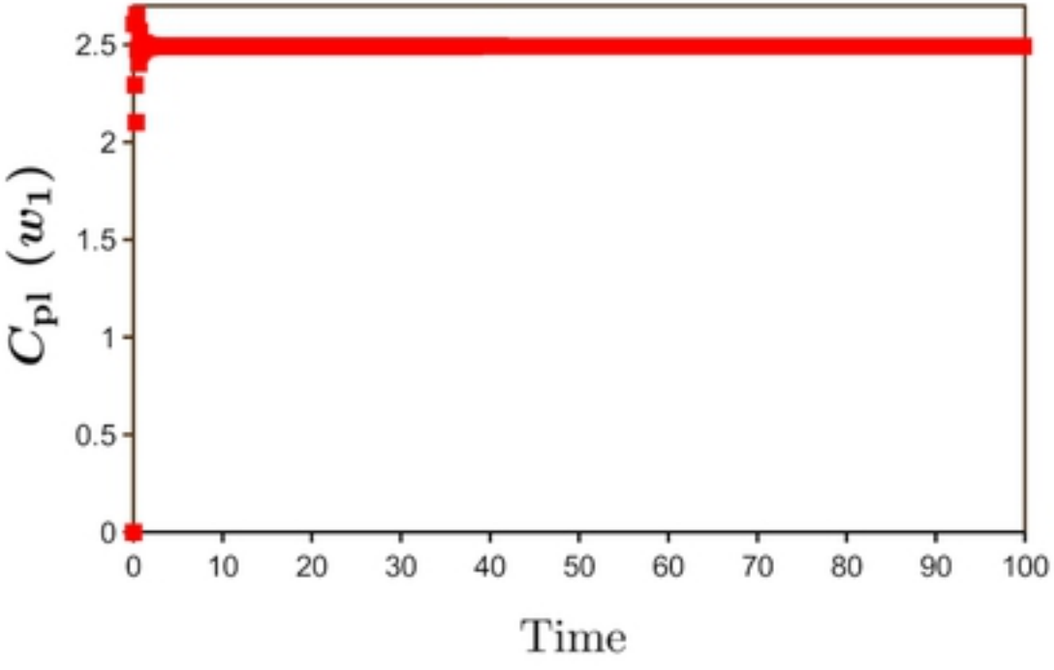

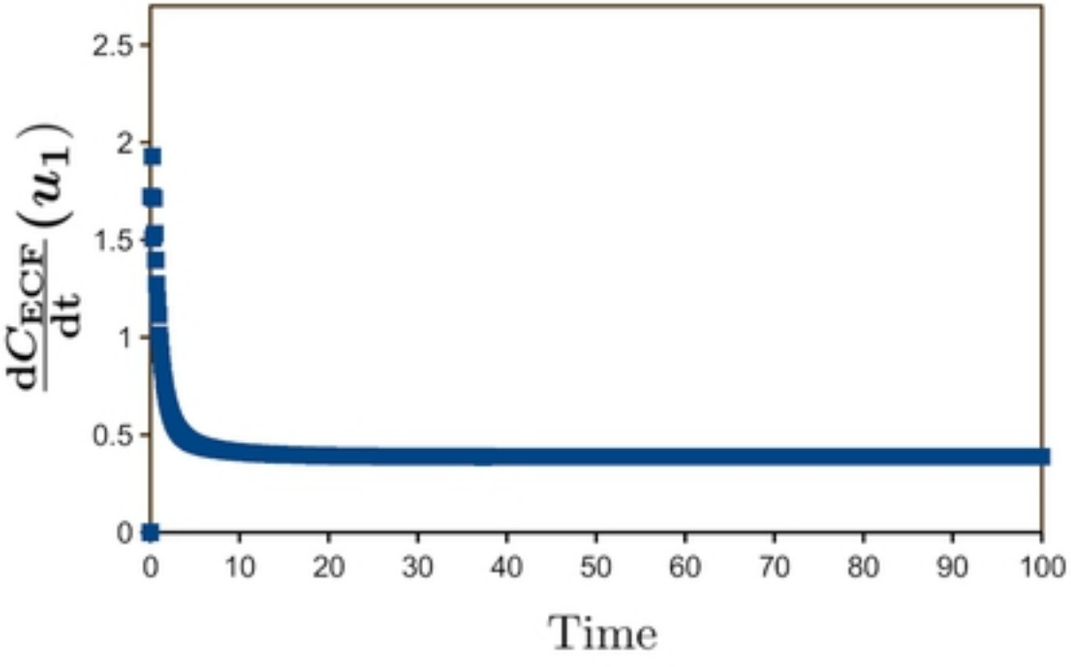

Supplementary Figure 2

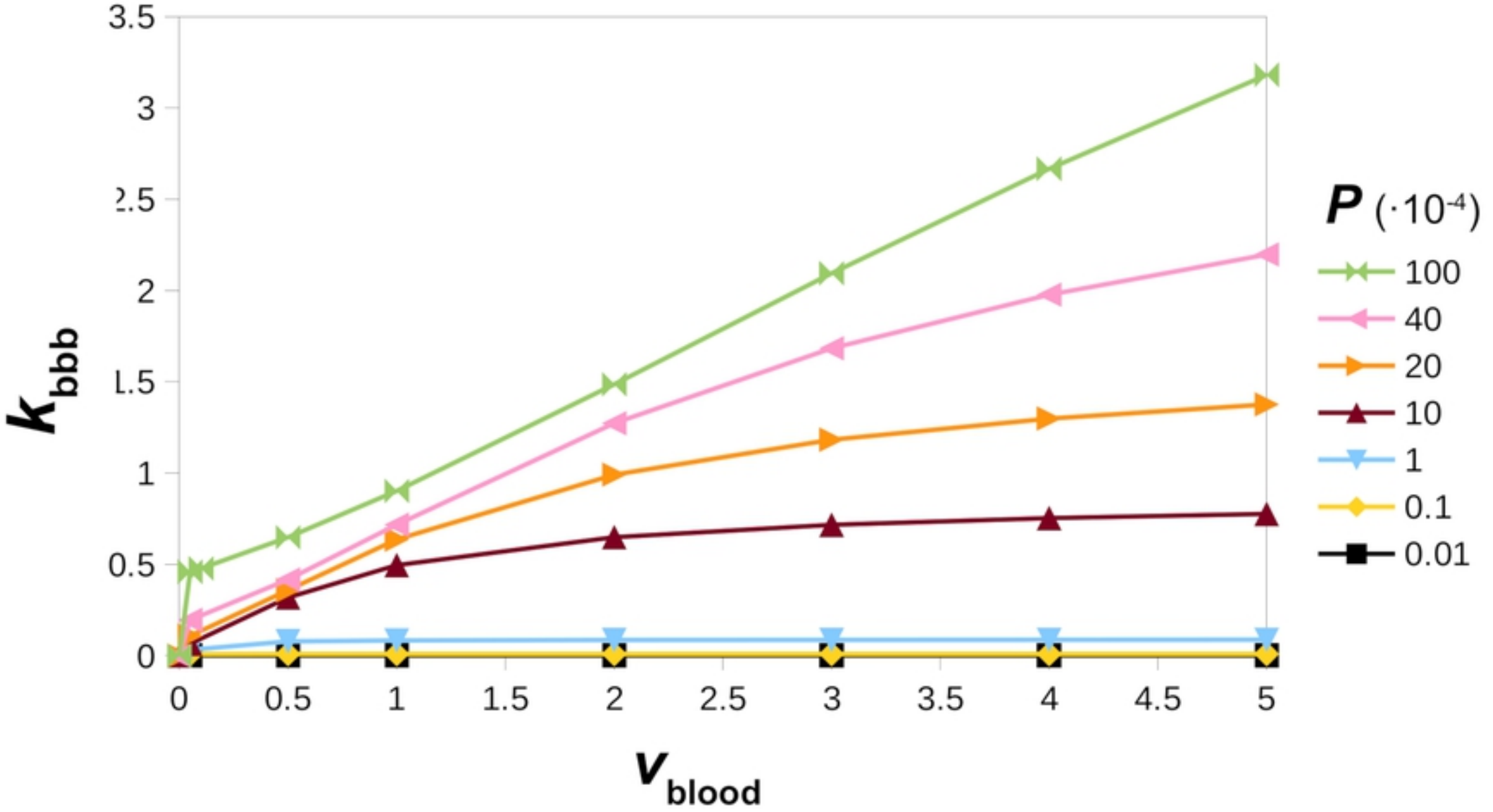

Supplementary Figure 3